

Annual Report 2019

Laboratory of Environmental Chemistry

On the cover page:

Probing the inside of microscopic particles. The X-ray image shows the iron oxidation state in aerosol particles in an environmental micro-reactor undergoing reaction with ozone, which only occurs near the particle surface at low relative humidity. Red and blue colours are more and less oxidized iron, respectively. Quantitative spatial profiles of the reaction over time with $0.035 \times 0.035 \mu\text{m}$ pixel resolution were derived.

Please see report on p. 7.

PAUL SCHERRER INSTITUT



Annual Report 2019

Laboratory of Environmental Chemistry

Editors

M. Schwikowski, M. Ammann

Paul Scherrer Institut

Laboratory of Environmental Chemistry

5232 Villigen PSI

Switzerland

Phone +41 56 310 25 05

www.psi.ch/luc

Reports are available: www.psi.ch/luc/annual-reports



TABLE OF CONTENT

Editorial	1
Surface Chemistry	
MIXING STATE AND HYGROSCOPICITY OF URBAN HAZE PARTICLES Y. Zhu, Z. Wu, J. Dou, U. K. Krieger, P. A. Alpert, M. Ammann	3
MIXING STATES OF AEROSOL PARTICLES IN URBAN HAZE S. Yang, F. Duan, K. He, P. A. Alpert, M. Ammann	4
ACID AND REDUCTIVE DISSOLUTION OF Fe AT THE FERRIHYDRITE SURFACE A. Boucly, L. Artiglia, H. Yang, J. P. Gabathuler, Y. Manoharan, M. Ammann	5
MULTIPHASE PHOTOCHEMICAL CONTROLS ON AEROSOL GROWTH J. D. Raff, P. A. Alpert, M. Ammann, T. Schaefer, H. Herrmann, S. S. Steimer, S. Yang, J. Dou, U. K. Krieger	6
MODELING REACTION AND MOLECULAR DIFFUSION IN SINGLE PARTICLES P. A. Alpert, P. Corral Arroyo, J. Dou, U. K. Krieger, S. S. Steimer, J.-D. Förster, F. Ditas, C. Pöhlker, S. Rossignol, M. Passananti, S. Perrier, C. George, M. Shiraiwa, T. Berkemeier, B. Watts, M. Ammann	7
NANOPLASTIC DEGRADATION UNDER ENVIRONMENTAL CONDITIONS M. Passananti, P. A. Alpert, P. Corral Arroyo, S. Yang, K. Witte, B. Watts, M. Ammann, A. Bianco, F. Sordello, D. V. Vione, J. Dou, U. K. Krieger	8
TOWARDS FAST AND ULTRAFast IODINE CHEMISTRY IN THE LIQUID PHASE Y. Uemura, M. Ammann, D. J. Suckow, M. Nachtegaal, C. Milne	9
INVESTIGATION OF BROMINE SPECIES AT THE LIQUID-GAS INTERFACE L. Artiglia, S. Chen, A. Boucly, H. Yang, I. Gladich, M. Ammann	10
CATIONIC AND ANIONIC SURFACTANTS AFFECT SURFACE BROMIDE S. Chen, L. Artiglia, H. Yang, A. Boucly, A. Laso, M. Ammann	11
A CATIONIC SURFACTANT ACCELERATES BROMIDE OXIDATION S. Chen, J. Edebeli, M. Ammann	12
TEMPERATURE DEPENDENCE OF THE STRUCTURE OF LIQUID WATER J. P. Gabathuler, H. Yang, A. Boucly, L. Artiglia, A. Laso, M. Ammann, T. Bartels-Rausch	13
WATER ORGANISATION NEAR SURFACE ACTIVE ORGANICS H. Yang, L. Artiglia, J. P. Gabathuler, A. Boucly, S. Chen, M. Ammann	14
X-RAY SPECTROMICROSCOPIC INVESTIGATION OF ICE FORMING PARTICLES P. A. Alpert, A. Boucly, A. Laso, M. Ammann, C. Padeste, S. Finizio, B. Watts	15
WATER ORGANISATION ON SILVER IODIDE SURFACES H. Yang, L. Artiglia, J. P. Gabathuler, A. Boucly, S. Chen, M. Ammann	16
MOLECULAR STRUCTURE OF WATER AT THE AIR-ICE INTERFACE J. P. Gabathuler, H. Yang, A. Boucly, L. Artiglia, A. Laso, M. Ammann, T. Bartels-Rausch	17
HOW TO KEEP NITRATE STABLE UNDER AN X-RAY BEAM Y. Manoharan, J. P. Gabathuler, H. Yang, A. Boucly, L. Artiglia, M. Ammann, T. Bartels-Rausch	18
WHAT DOES SNOW METAMORPHISM DO TO ITS CHEMICAL COMPONENTS? S. E. Avak, T. Bartels-Rausch, J. Edebeli, A. Eichler, M. Schneebeli, J. C. Trachsel	19
MAJOR IONS AND TRACE ELEMENTS IN SNOW FROM NORTHEASTERN CHINA H. Xue	20

Analytical Chemistry

ALTERING OF THE STABLE ISOTOPE SIGNAL IN AN ALPINE SNOW PACK J. C. Trachsel, F. Aemisegger, A. Eichler, S. Brütsch, T. Bartels-Rausch, S. E. Avak, J. Edebeli, M. Schneebeli.....	21
SNOW ACCUMULATION STUDIES IN THE CENTRAL KARAKORAM A. R. Groos, S. Erlwein, C. Mayer, A. Lambrecht, S. Brütsch, A. Eichler, M. Schwikowski.....	22
SIMILAR FIRN CHARACTERISTICS AFTER 5 DECADES ON ABRAMOV GLACIER M. Kronenberg, A. Eichler, S. Brütsch, M. Schwikowski, M. Hoelzle, H. Machguth.....	23
LIGHT ABSORBING IMPURITIES IN THE OLIVARES BASIN, CENTRAL CHILE M. Barandun, A. Rivera, B. Grobety, L. Fang, S. Köchli, K. Naegeli, M. Schwikowski.....	24
CARBONACEOUS AEROSOL TRENDS AND SOURCES FROM AN ALPINE ICE CORE L. Fang, C. Fang, S. Henne, S. Szidat, M. Schwikowski, T. M. Jenk.....	25
A NEW DATING TOOL FOR ALPINE ICE BASED ON DO ¹⁴ C L. Fang, T. Singer, S. Hou, T. M. Jenk, M. Schwikowski.....	26
MATCHING OF THREE DIFFERENT COLLE GNIFETTI ICE CORES T. Singer, A. Rieder, S. Brütsch, T. M. Jenk, P. Nalivaika, L. Fang, A. Eichler, M. Schwikowski.....	27
THE ADAMELLO ICE CORE – DATING WITH A TWIST T. M. Jenk, M. Schwikowski, V. Maggi, D. Festi.....	28
THE AGE OF ICE OF RHONE GLACIER – ICE FLOW MODELING AND ¹⁴ C DATES J. Morgenthaler, T. M. Jenk, G. Juvet, M. Schwikowski, A. Bauder.....	29
TOWARDS CROSS-DATING OF TWO ICE CORES FROM THE MONGOLIAN ALTAI P. Nalivaika, L. Marti, T. Singer, S. Brütsch, T. M. Jenk, M. Schwikowski, A. Eichler.....	30
CHERNOBYL HORIZON IN A CENTRAL ASIAN ICE CORE A. Eichler, M. Kronenberg, S. Brütsch, M. Rüthi, M. Heule, M. Schwikowski, H. Machguth, M. Hoelzle.....	31
DETERMINING THE AGE OF THE ICE IN THE MURTÈL ROCK GLACIER V. Bella, A. Cicoira, K. Gärtner-Roer, A. Vieli, T. M. Jenk, M. Schwikowski.....	32
THE INFLUENCE OF ACIDIFICATION TIME ON TRACE ELEMENT ANALYSIS T. S. Münster, T. M. Jenk, C. J. Huber, A. Eichler, P. Nalivaika, M. Schwikowski.....	33
List of Publications.....	34
Affiliation Index.....	36

EDITORIAL

Compared to what we are facing now with the Corona lockdown, the year 2019 was a normal one for our Laboratory of Environmental Chemistry, with exciting scientific activities, resulting in overall 24 papers in peer-reviewed scientific journals. I just want to mention here two highlights. For the first time internal concentration gradients in chemical components in viscous aerosol particles were observed directly using X-ray spectromicroscopy at the SLS PolLux endstation (Alpert et al., 2019, see cover page). This implies that atmospheric chemical reactions in particles can be significantly slowed and that chemical inhomogeneities may persist when diffusion of molecules is slow. This may extend the life time of aerosol particle or of toxic compounds therein. Further, a new ice dating method based on ^{14}C in dissolved organic carbon (DOC) in glacier ice was developed, which has the advantages of being less prone to carbonate interference and requiring smaller amounts of ice compared to the water insoluble organic carbon fraction previously used for dating (Fang et al., page 26).

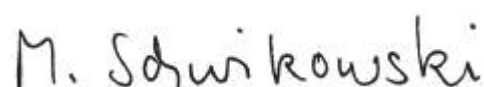
The year 2019 was also marked by a transition with two major SNF projects ending, the Sinergia project “Paleo fires from high-alpine ice cores” of the Analytical Chemistry group and the project “Microscale Distribution of Impurities in SnOw and Glacier Ice (MiSo)”, a collaborative work between both groups at LUC and the WSL-SLF. The seven PhD students involved successfully defended, among them Sven Avak at the University of Bern in 2019. With new projects starting, we welcomed six PhD students and two Postdocs at LUC in 2019. In addition, Markus Ammann’s SNF proposal on reactive oxygen species got funded and will begin in 2020 – my congratulation!

We are extremely pleased that Luca Artiglia, scientist

in the Surface Chemistry Group, whom we share with the Laboratory of Catalysis and Sustainable Chemistry (LSK) was awarded tenure at PSI. Luca is responsible for running the ambient pressure photoemission endstation at the in situ spectroscopy (ISS) beamline at SLS. Since 2019, this endstation has become open to the international user community. Colleagues from the University of Gothenburg were the first to make use of this opportunity in the environmental science context, already resulting in a first publication. Moreover, Sandra Brügger, PhD student in the Paleoecology group at the University of Bern, reconstructed past vegetation changes by analysing pollen and charcoal in ice cores in the frame of the Sinergia paleo fire project and received the prestigious “Prix de Quervain” for High Altitude Research awarded by the Swiss Committee on Polar and High Altitude Research for her work. Congratulations to both of them!

Our LUC excursion took us to Davos, where we visited the Physical Meteorological Observatory PMOD, enjoyed some beer tasting at the brewery Monstein, and hiked from there to Sertig Dörfli. We concluded the year with the Christmas cooking and eating activity at mein-kuechenchef.ch – from the field to the plate – without food waste.

I hope you enjoy reading our LUC annual report and apologize for the late publication, which is due to Corona-related work overload.



Margit Schwikowski

MIXING STATE AND HYGROSCOPICITY OF URBAN HAZE PARTICLES

Y. Zhu, Z. Wu (PKU), J. Dou, U. K. Krieger (ETHZ), P. A. Alpert, M. Ammann (PSI)

Quantifying how atmospheric particles interact with water vapor is critical to understand their role in atmospheric chemistry, Earth’s climate and human health. We present a novel method to measure single atmospheric particle hygroscopicity while characterizing elemental and carbon functional group composition.

Atmospheric aerosols, solid or liquid particles suspended in the atmosphere, range in size from 1 nm to $>100\ \mu\text{m}$ and come from a wide variety of sources [1]. Atmospheric particles are chemically complex and can contain hydrophobic carbonaceous material such as soot and fresh anthropogenic emissions, but also hygroscopic salts such as sulfate and nitrate [2]. The immense complexity of aerosol chemical composition and atmospheric processes hinder realistic prediction of the prevailing particle morphology during its atmospheric life cycle, and how critical particle properties would evolve [3]. As such, aerosols have a wide range of chemical and physical properties that require detailed analytical measurements to be fully described [4].

We use X-ray spectromicroscopy to quantify how organic matter, inorganic matter, and black carbon is mixed in individual particles from an anthropogenic aerosol particle population with well-characterized meteorological conditions and bulk chemical composition. Also, we subjected ambient samples to a high relative humidity, $\text{RH}=70\%$, and probed particles that do and do not take up water to see how their mixing state changes. Particles collected on a copper grid at the PKU supersite in Beijing, China, on 1st Oct. 2019 at 17:04 (GMT+8) were mounted in the PolLux in-situ cell, a custom built environmental microreactor.

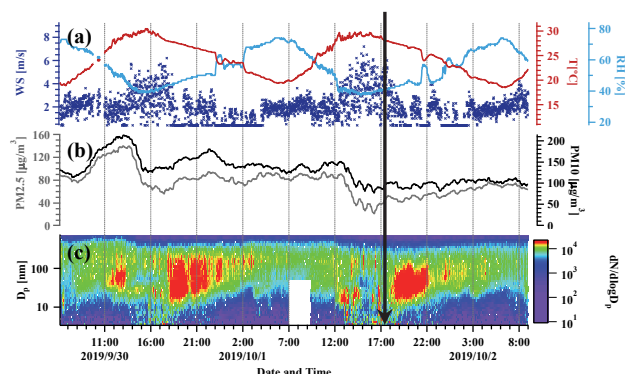


Fig. 1: Time series of (a) meteorological parameters including wind speed, ambient temperature and RH, (b) particulate matter mass concentrations, and (c) particle number size distribution from 3 to 700 nm measured at PKU supersite. The sample was collected at the time indicated by the arrow.

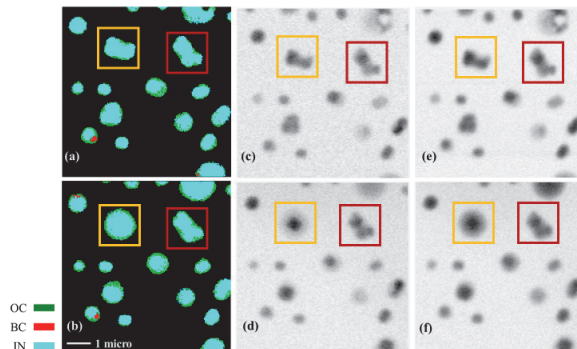


Fig. 2: Random sample of ~ 15 particles showing (a-b) sub-particle carbon speciation and (c-f) water uptake reflected by the increasing oxygen absorption. Colors indicate dominant type: OC-Organic Carbon, BC-Black Carbon and IN-Inorganic. (a), (c), (e) Elemental mapping under dry condition. (b), (d), (f) Elemental mapping under 70 % RH. Fig. 2c & Fig. 2d were acquired at 520 eV, which is the pre-edge of oxygen. Fig. 2e & Fig. 2f were acquired at 550 eV, which is post-edge of oxygen. Yellow and red squares are example particles that are hygroscopic and non-hygroscopic, respectively.

Fig. 1 shows the ambient conditions during the sampling time of atmospheric particles collected at PKU supersite. Fig. 2 shows an example of carbon speciation and oxygen mapping on particles, although our full dataset comprises hundreds of them. STXM/NEXAFS measurements will provide insights into the evolution of particle morphology and chemical properties when air pollution builds up. We are currently addressing the question, why aerosol populations have a multi-modal hygroscopicity distribution as seen in Fig. 1. Our data is invaluable to directly probe the chemical complexity of individual particles and their hygroscopicity.

We acknowledge funding from the National Natural Science Foundation of China (Grant No. 41875149) and the Swiss National Science Foundation (Grant 163074).

- [1] W. C. Hinds, in *Aerosol technology: Properties, behavior, and measurement of airborne particles* (1982)
- [2] B. R. Bzdek and J. P. Reid, *J. Chem. Phys.*, **147**, 220901 (2017).
- [3] K. Gorkowski, N. M. Donahue and R. C. Sullivan, *Chem.*, **6**, 204-220 (2019).
- [4] A. P. Ault and J. L. Axson, *Anal. Chem.*, **89**, 430-452 (2017).

MIXING STATES OF AEROSOL PARTICLES IN URBAN HAZE

S. Yang (THU & PSI), F. Duan, K. He (THU), P. A. Alpert, M. Ammann (PSI)

Oligomers ($m/z > 200$) are a significant component of atmospheric SOA and were evidently produced via multiphase processes in high relative humidity conditions. We propose to investigate mixing states and quantify the critical role of relative humidity on phase separation in single ambient oligomer-containing particles by STXM/NEXAFS.

Secondary Organic aerosols (SOA) comprise a large fraction of $PM_{2.5}$ mass concentrations and they are one of many driving factors of extreme haze, affecting visibility and impairing human health, especially in the Northern China Plain. Laboratory studies have found that oligomers could contribute to 22-50 % of SOA mass and 80-90 % of total detected molecular ion peaks, which confirmed oligomerization was a significant atmospheric process for SOA formation [1]. The campaign in Beijing using matrix-assisted laser desorption ionization time of flight mass spectrometry (MALDI-TOF-MS) observed oligomers and found out oligomers were significant to OA in Beijing and evidently produced via multiphase processes under high relative humidity conditions [2]. Meanwhile, it is well known that SOA undergoes liquid-liquid phase separation (LLPS) but it has never been directly observed in single ambient aerosol particles.

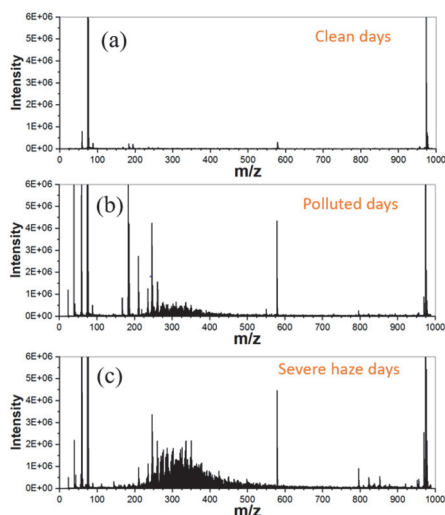


Fig. 1: LDI-TOF-MS spectra of oligomers with (a) $PM_{2.5}$ at $23.2 \mu\text{g m}^{-3}$; (b) $PM_{2.5}$ at $168.6 \mu\text{g m}^{-3}$; (c) $PM_{2.5}$ at $318.0 \mu\text{g m}^{-3}$;

We aimed to probe atmospheric aerosol chemical morphology and to acquire mixing states and phase transition information of individual aerosol particles containing oligomers in urban haze events. We will investigate particle samples before, during and at the peak of a pollution event and pair our results with online observations of inorganic and organic aerosol, in particular, oligomers. We will observe whether organic matter in

particles that readily takes up water exhibits very different functionality and phase separation compared to other particles in our aerosol populations. In particular, we aim to be the first to observe liquid-liquid phase separation in single ambient particles by mapping carbon at high RH.

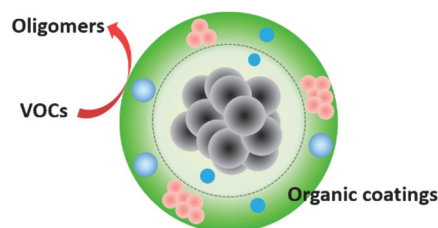


Fig. 2: Conceptual graph of LLPS in an individual particle

Size-resolved aerosol samples collected in Beijing will be analyzed by spatial resolution of scanning X-ray microscopy (STXM) in combination with near edge X-ray absorption fine structure spectroscopy (NEXAFS) [3]. We will acquire i) representative C-N-O spectra, ii) maps and mixing state of particles, and iii) quantitative information on the critical role of relative humidity on phase separation and water uptake when exposing our oligomer-containing particles to water vapor in the Pol-Lux-in-house environmental cell.

The results will give statistically information about particle mixing state for aerosol with different total oligomer content, humidity history and pollution levels. We will be able to claim if liquid-liquid phase separation occurs in single ambient aerosol particles and if there is a trend with oligomer formation and mixing state differences.

We acknowledge funding from the National Science and Technology Program of China (grant 2017YFC0211601), the National Research Program for Key Issues in Air Pollution Control (DQGG0103).

- [1] M. Kalberer et al., *Science*, **303**, 1659-1662 (2004).
- [2] F. K. Duan et al., *Environ. Pollut.*, **218**, 289-296 (2016).
- [3] R. C. Moffet et al., *Analytical Chemistry*, **82**, 7906-7914 (2010).
- [4] O'Brien et al., *Environ. Sci. Technol.*, **49**, 4995-5002 (2015).

ACID AND REDUCTIVE DISSOLUTION OF Fe AT THE FERRIHYDRITE SURFACE

A. Boucly (PSI LEC & LUC), L. Artiglia (PSI LSK & LUC), H. Yang, J. P. Gabathuler, Y. Manoharan (PSI & ETHZ), A. Laso, M. Ammann (PSI)

The influence of acids on the leaching of iron from ferrihydrite (an iron(III) oxy-hydroxide structure), has been monitored *in situ* through electron yield Near Edge X-ray Absorption Fine Structure (NEXAFS) spectroscopy and X-ray Photoelectron Spectroscopy (XPS).

Ferrihydrite is a metastable nanoaggregate Fe(III)-oxy-hydroxide material (1-10 nm particle) omnipresent in nature with a high specific surface area offering a high number of accessible sites for adsorption and reaction [1-2]. It has no clear structure, no fixed composition and is metastable [1], and it slowly evolves into either goethite or hematite. It is also considered to be the main source of bio-available iron [3] (iron that can be leached from the mineral and absorbed by organisms) and thus has a huge impact on marine life. Ferrihydrite mainly comes from dust particles emitted from deserts, such as the Sahara. Thus, ferrihydrite can have an impact both on atmospheric chemistry as an aerosol particle and on the ocean when deposited. There is a clear lack of electron spectroscopy experiments on ferrihydrite due to its non-conductive nature. Yet it is part of the important Fe(II)/Fe(III) redox couple, which interacts with different other redox active systems, such as reactive oxygen species (ROS) and secondary organic compounds associated with mineral dust aerosol particles. Here we present an extract from an XPS and NEXAFS experiment to study the iron leaching and modification of the ferrihydrite surface.

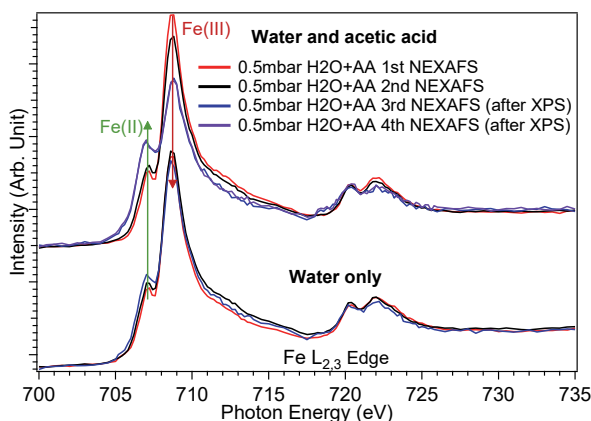


Fig. 1: Fe $L_{2,3}$ Edge NEXAFS spectra of ferrihydrite with only water vapor (a) and with 0.01 mbar of acetic acid (b) both acquired at RH=90 % (-26.3 °C under 0.5 mbar). Red and black lines correspond to NEXAFS spectra taken before XPS measurement, blue and purple correspond to NEXAFS spectra taken after XPS.

During those experiments, various acids have been used such as citric acid, ascorbic acid and acetic acid. The results presented here will focus on acetic acid. This experiment shows the enhanced dissolution of iron in

presence of gas phase acetic acid compared to just pure water vapor. To distinguish the iron leached from the solid mineral oxide from the one still present as part of ferrihydrite we use the susceptibility of hydrated Fe(III) species to be reduced to Fe(II) under the X-ray beam. In the spectra, the Fe(III) corresponds to the iron still present in the intact ferrihydrite structure, while the Fe(II) represents the leached (and hydrated) Fe.

Fig. 1 shows the Fe $L_{2,3}$ Edge NEXAFS spectra of ferrihydrite in presence of 0.5 mbar of water vapor only (bottom) and in combination with 0.01 mbar of acetic acid (top) at -26.3 °C (90 % relative humidity). When we consider the experiment with water only we observe that the feature corresponding to Fe(II) does not increase much between two NEXAFS measurements (red and black curve), it only slightly increases after XPS measurements and the concomitant X-ray exposure (between black and blue curve). As with pure water, the experiment done with the addition of acetic acid shows only a small difference between the first two NEXAFS spectra. Yet after the XPS measurement, we observe that the feature corresponding to Fe(II) has increased a lot (black to blue curve) compared to the experiment done with water only. A complete XPS characterization involves a longer acquisition time compared to a NEXAFS spectrum, giving more time for the leaching to occur. In presence of acetic acid, this is accelerated and thus more apparent. This experiment shows that a small amount of acid can greatly enhance the leaching of iron at the surface of ferrihydrite, iron that is now able to react with species in its environment. This is interesting from the aerosol particle point of view as this available iron can be converted back to Fe(II) through photochemical processes forming the redox couple and thus be able to do redox reactions with other airborne species such as H_2O_2 or secondary organic compounds.

Funding via the Interlaboratory Postdoc program of the ENE division is appreciated.

- [1] U. Schwertmann et al., *J. Colloid Interface Sci.*, **209**, 215-223 (1999).
- [2] T. Hiemstra et al, *Geochim. Cosmochim. Acta*, **105**, 316-325 (2013).
- [3] C. Rodriguez-Navarro et al., *Atmos. Chem. Phys.*, **18**, 10089-10122 (2018).

MULTIPHASE PHOTOCHEMICAL CONTROLS ON AEROSOL GROWTH

J. D. Raff (Indiana Univ.), P. A. Alpert, M. Ammann (PSI), T. Schaefer, H. Herrmann (TROPOS), S. S. Steimer (Univ. Basel), S. Yang (THU/PSI), J. Dou, U. K. Krieger (ETHZ)

Organic photochemistry occurring within aerosols generates reactive oxygen species (ROS) that enhance reactive uptake of volatile organic compounds and promotes particle growth. Iron particles scavenge ROS and shut down particle growth.

Traditional models of secondary organic aerosol (SOA) formation view particle growth as due to the absorption of semi-volatile organic photoproducts into preexisting aerosol mass. Less is known about how chemistry occurring *within* aerosol droplets drives reactive uptake of gases into the bulk aerosol phase. To address this knowledge gap, we studied the uptake of α -pinene onto aerosols comprised of ammonium sulfate $[(\text{NH}_4)_2\text{SO}_4]$ and anthraquinone-2-sulfonate (AQ2S), a triplet state chromophore widely used to model the photochemistry of chromophoric dissolved organic matter. Aerosols were nebulized into a 19 m³ Teflon chamber containing 50 ppbV of α -pinene. After a brief equilibration time, UV-visible lights ($300 < \lambda < 400$ nm) irradiated the chamber to initiate aerosol photochemistry.

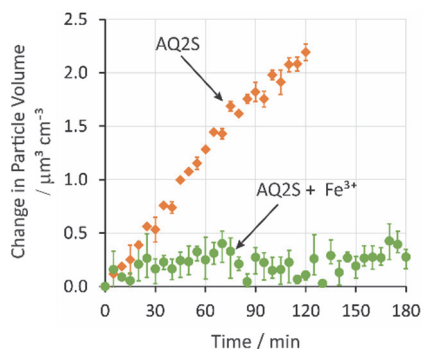


Fig. 1: Particle volume measured by scanning mobility particle sizer during aerosol chamber experiments containing gaseous α -pinene and seed aerosol comprised of $(\text{NH}_4)_2\text{SO}_4$ and the indicated components.

Fig. 1 shows that UV-visible irradiation induces particle growth on seed aerosol particles containing $(\text{NH}_4)_2\text{SO}_4$ and organic chromophores, relative to the experiments where α -pinene is irradiated in the presence of the pure $(\text{NH}_4)_2\text{SO}_4$ seed aerosol. Enhanced particle growth in the presence of chromophores indicates reactive uptake of α -pinene into the aerosol phase, which is driven by ROS formed via the reaction of O_2 with excited state chromophores. Addition of Fe^{3+} shuts this chemistry down, effectively limiting particle growth. To explore this effect at the single particle level, aerosols were collected from chamber experiments and analyzed via near edge X-ray absorption fine structure spectroscopy (NEXAFS).

Fig. 2 shows NEXAFS spectra of seed particles, and those particles exposed to α -pinene under UV light with and without Fe^{3+} . AQ2S shows two peaks at 284.4 and

284.8 eV associated with the quinone ring structure [1]. Another peak at 286.3 eV is associated with a phenol group [1], indicating the presence of semi- or hydroquinones [2]. After exposure to α -pinene and UV light, particles with and without Fe^{3+} were entirely dominated by three peaks at 285.1, 286.7 and 288.6 eV indicative of unsaturated carbon, hydroxyl and carboxyl functions, respectively. Spectra are similar to those of α -pinene SOA generated from gas phase OH chemistry [3], indicating similar α -pinene oxidation pathways occur in the bulk aerosol phase. Consistent with chamber experiments in Fig. 1, we observed significantly less SOA material on particles containing Fe^{3+} . Together, the results show that reactive uptake is controlled by a competition between ROS sources (organic chromophores) and sinks (Fe^{3+} and Fe^{2+}), with implications for understanding the drivers of particle growth when mineral dust is present.

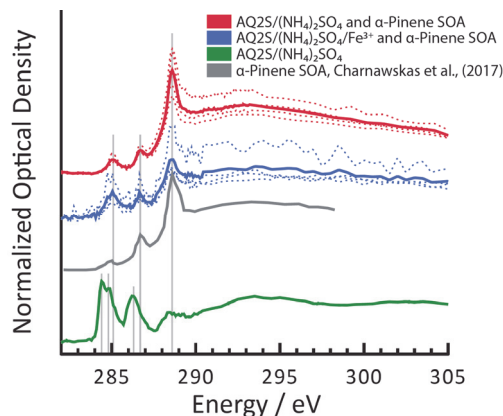


Fig. 2: Normalized NEXAFS spectra of indicated aerosol particles exposed to α -pinene under UV light. Solid lines are averages of individual particles, which are dotted lines. Spectra are background subtracted and normalized to the area between 305-320 eV. Spectra of α -pinene SOA from literature is shown [3].

Funding for this work was provided by EUROCHAMP-2020 (Project LEAK-LACIS-002-2017), the Atmospheric Chemistry Department (ACD) at the Leibniz Institute for Tropospheric Research (TROPOS), and the Swiss National Science Foundation (Grant 163074).

- [1] R. C. Moffet et al., in *Fundamentals and Applications in Aerosol Spectroscopy*, CRC Press, 419-462 (2010).
- [2] N. K. Scharko et al., *Environ. Sci. Technol.*, **51**, 9633-9643 (2017).
- [3] J. C. Charnawskas et al., *Faraday Discuss.*, **200**, 165-194 (2017).

MODELING REACTION AND MOLECULAR DIFFUSION IN SINGLE PARTICLES

P. A. Alpert, P. Corral Arroyo (PSI), J. Dou, U. K. Krieger (ETHZ), S. S. Steimer (Univ. Basel), J.-D. Förster, F. Ditas, C. Pöhlker (MPIC), S. Rossignol (Aix-Marseille Univ.), M. Passananti (Univ. Torino), S. Perrier, C. George (IRCELYON, CNRS), M. Shiraiwa (Univ. California, Irvine), T. Berkemeier (MPIC), B. Watts (PSI LSC), M. Ammann (PSI)

Accurate prediction of aerosol particle multiphase chemical degradation initiated by trace gases highly depends on diffusion of reactants and solubility of the reactive trace gas. We used the kinetic multi-layer model for aerosol surface and bulk chemistry (KM-SUB) to put accurate constraints on Henry’s law and diffusion coefficients, leading to more accurate predictions.

The majority of atmospheric aerosol particles are composed of organic matter. It has been shown that when air is sufficiently cold and dry, ambient particles are likely to be in a highly viscous phase state. As a consequence, particles will not be well mixed during multiphase chemical reactions that begin at a particle’s surface.

In our recent study [1], we were the first to observe gradients in condensed-phase reactant concentration throughout particles as the result of diffusion and chemical reaction limitations, termed chemical gradients. We investigated the reaction between O_3 and aerosol particles composed of xanthan gum and $FeCl_2$ and observed the in situ chemical reaction that oxidized Fe^{2+} to Fe^{3+} using X-ray spectromicroscopy. Iron oxidation state of particles as small as 0.2 μm in diameter were imaged over time with a spatial resolution of tens of nanometers. Concentric 2-D column integrated profiles of the Fe^{2+} fraction out of the total iron, α , were derived and demonstrated that particle surfaces became oxidized while particle cores remained unreacted at RH=0-20%. At higher RH, chemical gradients evolved over time, extended deeper from the particle surface, and Fe^{2+} became more homogeneously distributed.

We have employed the KM-SUB model [2] to infer values of the Henry’s law coefficient for ozone, H_{O_3} , the diffusion coefficient of ozone, D_{O_3} , and the diffusion coefficient of iron, D_{Fe} , to reproduce observed profiles in α over a wide range of RH and gas phase O_3 concentration. Briefly, this model solves the system of nonlinear differential equations for the rate of change of O_3 and Fe^{2+} with time in prescribed layers with defined thickness. It accounts for O_3 accommodation and absorption, the O_3 and Fe^{2+} diffusion from the surface and within bulk layers and finally, the chemical loss of O_3 and Fe^{2+} .

We investigated the sensitivity of the model to input parameters using our dataset with hundreds of particles at RH=40%. When varying only D_{O_3} and H_{O_3} , the sum of the squared residuals (RSS) surface in Fig. 1A clearly shows a high correlation and a clear minimum could not be determined. This is due to our reactive system being in the regime of reacto-diffusive limitation [2-4].

We also determined the sensitivity of the model when all three parameters were allowed to vary. RSS contours are shown in Fig. 1B as a function of D_{Fe} and the product $H_{O_3}\sqrt{D_{O_3}}$. We found multiple local minima in this parameter space, however one clear global minimum was identified. Fitted parameters are the black crosses in Figs. 1 and 2. From this sensitivity analysis we derive two conclusions. The first is that our observed 2-D profiles of α were a good enough constraint that a unique value of D_{Fe} could be found to minimize the residuals. Second, we found that although D_{O_3} and H_{O_3} were correlated, their product $H_{O_3}\sqrt{D_{O_3}} = -7.7$ seen as the dashed line in Fig. 1, could be constrained.

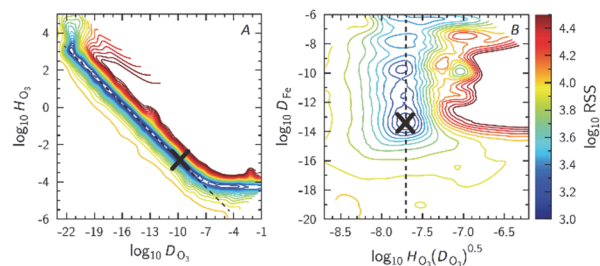


Fig. 1: Model parameters sensitivity in KM-SUB. (A) D_{O_3} and H_{O_3} were varied while keeping D_{Fe} constant. (B) All three parameters were varied simultaneously. The product of $H_{O_3}\sqrt{D_{O_3}} = -7.7$ is the dashed line in both panels. Color contours are the sum of the squared residual values (RSS) between model and observations.

Accurate chemical evolution of highly viscous atmospheric aerosol should include accurate knowledge of solubility and diffusion. We suggest that highly detailed and direct measurements of internal and near-surface (nanometer scale) observations together with kinetic model simulations should further constrain future parameter derivation.

We acknowledge funding from the Swiss National Science Foundation (Grant 163074).

- [1] P. A. Alpert et al., *Phys. Chem. Chem. Phys.*, **21**, 20613-20627 (2019).
- [2] T. Berkemeier et al., *Phys. Chem. Chem. Phys.*, **18**, 12662-12674 (2016).
- [3] S. S. Steimer et al., *Atmos. Chem. Phys.*, **14**, 10761-10772 (2014).
- [4] S. S. Steimer et al., *Phys. Chem. Chem. Phys.*, **17**, 31101-31109 (2015).

NANOPLASTIC DEGRADATION UNDER ENVIRONMENTAL CONDITIONS

M. Passananti (Univ. Torino, Univ. Helsinki), P. A. Alpert, P. Corral Arroyo (PSI), S. Yang (THU & PSI), K. Witte, B. Watts (PSI LSC), M. Ammann (PSI), A. Bianco (Univ. Helsinki), F. Sordello, D. V. Vione (Univ. Torino), J. Dou, U. K. Krieger (ETHZ)

Weathering of nanoplastics induces chemical and physical changes, resulting in by-products released into the environment. We induced abiotic transformation of polystyrene (PS) nanoparticles in water and quantified product formation on particles and in the liquid phase.

Microplastics (MPs) and nanoplastics (NPs) are either directly emitted into the environment or formed by physical degradation of larger plastic debris. They are environmentally ubiquitous and persistent in the atmosphere, surface waters and soils. MPs and NPs in the environment undergo weathering, induced by mechanical abrasion, oxidation, UV radiation or microbiological activity. Oxidation and photo-oxidation becomes an important chemical degradation pathway when the size of plastic particles decreases, (i.e. $<2 \mu\text{m}$ in size), because reactivity is proportional to the surface to volume ratio [1]. It is important to note that NPs are not inert and can interact with chemical species present in the surrounding environment, including the adsorption of metals and other persistent organic pollutants [2]. These interactions can lead to unique reactive and photochemical pathways.

We used PS nanoparticles as a NP proxy, and quantified the release of degradation products to water under environmental conditions using electrospray ionization differential mobility analyser coupled with an atmospheric pressure interface time of flight (ESI-DMA-API-TOF). PS nanoparticles were immersed in distilled and deionized water with and without the presence of iron(II) and irradiated with UV light. The kinetics of iron(II) degradation and the change of total iron in solution were determined. Chemical changes of PS particles in terms of carbon and oxygen functionality and iron oxidation state were investigated with scanning transmission X-ray microscopy coupled to near-edge X-ray absorption fine structure spectroscopy (STXM/NEXAFS) [3].

A suspension of PS particles all having a diameter of 100 nm was exposed for 1 year (October 1st, 2018-October, 1st, 2019) on the rooftop of the Physicum building of the Kumpula campus in Helsinki. This suspension turned yellow upon exposure. Liquid phase analysis revealed the formation of carboxylic acids and aromatic compounds, some of which are toxic, such as phenol and benzene (see Figure 1). STXM/NEXAFS results showed a significant amount of organic matter with ketone and carboxylic functions being released to the aqueous phase.

These experiments show that NPs can be degraded in the environment and release organic matter to water, with possible consequences on carbon cycle and toxic contamination. NPs can perturb the natural photochemical equilibria, interacting with naturally occurring

species and/or modify the natural organic matter content due to the products release during degradation.

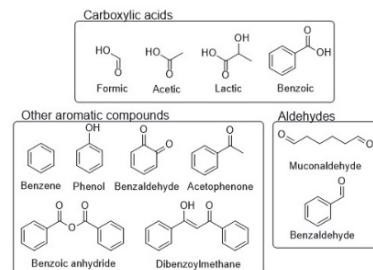


Fig. 1: Degradation products identified in the liquid phase after PS exposure to sunlight for one year.

When PS particles and iron were present in water together, iron(II) transitioned to iron(III) when irradiated in air. Fig. 2 shows that iron(II) rapidly degraded by 90 %, coinciding with an equal loss of total iron from the solution. This implies that it was adsorbed to the surface of PS particles. Indeed, we observed by STXM/NEXAFS analysis that iron was uniformly present on PS particles, mainly as iron(III).

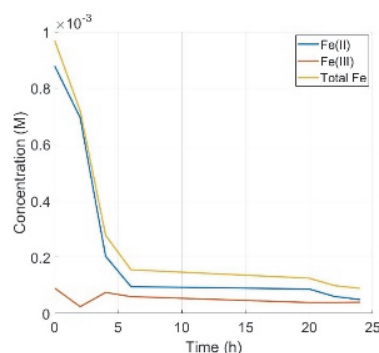


Fig. 2: Fe(II), Fe(III) and total iron concentration changes during irradiation of a suspension of PS nanoparticles in water.

We acknowledge funding from the University of Helsinki (Three-Year Research Grant) and the Swiss National Science Foundation (163074).

- [1] K. Mattsson et al., in *Microplastic Contamination in Aquatic Environments*, Elsevier, 379-399 (2018).
- [2] C.-B. Jeong et al., *Environ. Sci. Technol.*, **52**, 11411 (2018).
- [3] J. Raabe et al., *Rev. Sci. Instr.*, **79**, 113704 (2008).

TOWARDS FAST AND ULTRAFast IODINE CHEMISTRY IN THE LIQUID PHASE

Y. Uemura, M. Ammann (PSI), T. Lind, D. J. Suckow (PSI LRT), M. Nachttegaal (PSI ENE & LSF),
C. Milne (PSI PSD & LSF)

In this project, we would like to understand reaction mechanisms of organo-iodine compounds in the liquid phase, especially in water. Employing SwissFEL, which is an x-ray free electron laser, and Swiss Light Source (SLS), which is a synchrotron radiation facility, can address chemical reaction and dynamics over different time scales (ps ~ μ s).

Iodine compounds play important roles in environmental chemistry [1]. Organo-iodides coming from biologically active oceans undergo photolysis in the aqueous phase, leading to reactive iodine species in the gas phase, where they participate in ozone depleting catalytic cycles or are oxidized to climate relevant iodine oxide nanoparticles. Iodine is also an important element during severe accidents in nuclear reactors due to its volatility and high radiotoxicity. The suppression of the release of organic iodides from a power plant is a main issue in nuclear power plants (NPPs) safety. Organo-iodides such as methyl iodide (MI) or ethyl iodide (EI) are key intermediate compounds from reactions of reactive iodine species with organic materials, e.g., paints, used in containments, or also organic compounds in the environment. In contrast to the gas phase [2], the photodissociation of MI in the liquid phase has been rarely studied [3]. In the context above, the population and the fate of dissociation fragments in solutions against reaction time need to be understood.

In this project, we would like to understand fundamental processes related to photolysis of organo-iodide compounds in the liquid phase, especially in water, by using time-resolved x-ray absorption spectroscopy (XAS). XAS can provide the electronic state and geometrical configurations of an objective element. Since X-rays above 4000 eV have relatively long attenuation lengths in relevant materials, XAS can be observed in various kinds of phases. XAS can address the kinetics of fast chemical reactions in nanoseconds or microseconds combining pulsed lasers in synchrotron facilities. XAS can also address the photodissociation dynamics in picoseconds or sub-picoseconds regimes by employing X-ray free electron lasers (XFELs) as shown in Fig. 1 for the example of hematite. We would like to employ SwissFEL, which is an XFEL, and the Swiss Light Source (SLS), which is a synchrotron radiation facility, to observe photodissociation dynamics and follow-up reaction kinetics, respectively, with MI or EI.

Understanding the reaction mechanisms of organo-iodine compounds will give new insight into the production of iodine species in oceans and in the atmosphere and help to assess the distribution of iodine within different environmental compartments. It also helps in the understanding of the reactivity of iodine inside NPPs and in scrubbing devices after a nuclear accident. Pho-

todissociation mechanisms and kinetics of iodide compounds in water should be an essential part of developing new pathways to prevent the release of organo-iodine compounds.

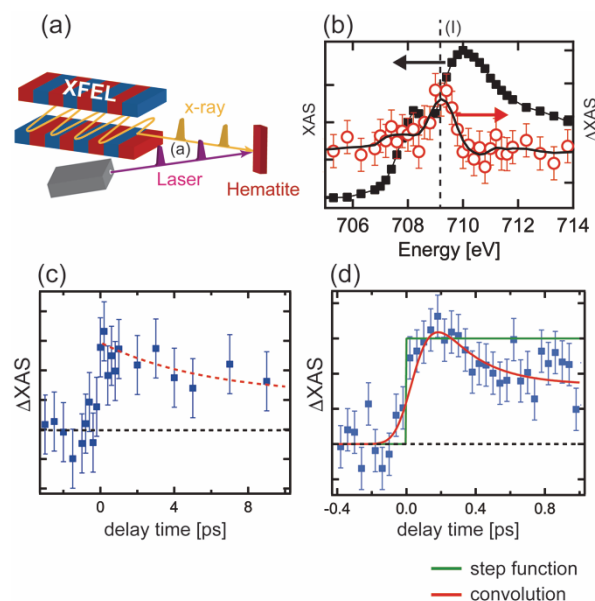


Fig. 1: pump probe XAS of hematite : (a) an illustration of the pump probe experiments in Pohang Accelerator Laboratory (PAL-XFEL) (b) Fe L_3 XAS of hematite (black) and difference XAS at a delaytime of 0.2 ps (red) (c) a kinetic trace at the energy point of 709 eV (denoted as (I) in (b)) (d) a kinetic trace at the energy point of 709 eV around the vicinity of 0 ps.^[4]

Y. Uemura is funded via the I-CROSS project at PSI co-funded by ENE, NES and PSD.

We acknowledge funding from the Swiss National Science Foundation (Grant no 188662). We also acknowledge European Research Council (ERC) under the European Union's Horizon 2020 research and innovation programme (Principal Investigator: Prof. Frank de Groot, grant agreement No 340279).

- [1] L. J. Carpenter et al. *Chem. Rev.*, **115**, 4015-4034 (2015).
- [2] A. R. Attar et al. *J. Phys. Chem. Lett.*, **6**, 5072-5077 (2015).
- [3] Y. Wang et al. *Chem. Phys. Lett.*, **633**, 126-131 (2015).
- [4] A. S. M. Ismail, Y. Uemura, F. M. F. de Groot et al. *Phys. Chem. Chem. Phys.*, advanced article (2020).

INVESTIGATION OF BROMINE SPECIES AT THE LIQUID-GAS INTERFACE

L. Artiglia (PSI LSK & LUC), S. Chen (PSI & ETHZ), A. Boucly (PSI LEC & LUC), H. Yang (PSI & ETHZ), I. Gladich (QEERI), M. Ammann (PSI)

The oxidation of halide ions with ozone in aqueous environments initiates the formation of molecular halogen compounds in the atmosphere. The goal of this work is to locate and characterize bromine-containing species dissolved in water by means of in situ spectroscopy and molecular dynamics calculations.

Halogen atoms are known to catalyze ozone depletion in the stratosphere and in the tropospheric boundary layer [1]. Ozone depletion events in the polar boundary layer correlate with a notable increment of bromine gas concentration [2]. This affects the global chemical balance in the atmosphere [3]. We have already investigated in situ the reaction between bromide ions and ozone, identifying for the first time an ozonide ($[\text{Br}\cdot\text{OOO}\cdot]$) pre-complex located at the liquid-gas interface [4]. However, a complete experimental and theoretical characterization of all the bromine-containing species potentially involved in the mechanism is still lacking. We made use of ambient pressure X-ray photoelectron spectroscopy (APXPS) to characterize the electronic state of the species dissolved in aqueous solutions and injected in the experimental chamber by means of a liquid microjet [5]. Such an approach allows the characterization of the liquid-vapor interface with high surface sensitivity and with limited beam-induced effects. The experiments were performed at the SIM beamline at the Swiss light source. The experimental results, combined with molecular dynamics (MD) calculations show the location and solvation environments of selected bromine-containing species.

Fig. 1 shows the Br 3d photoemission peaks of aqueous solutions of solutes where bromine has different oxidation states: -1 (Br^-), +1 (BrO^-) and +5 (BrO_3^-). The spectra were deconvoluted based on previous literature data [4] and the fitting parameters were constrained to get a reliable analysis. While the spectra of Br^- and of BrO_3^- display a single doublet, corresponding to a single oxidation state, the ones of BrO^- at different pH values have more than one component. This is due to the synthesis strategy, which envisages the disproportionation of bromine in an alkali solution (0.5 M NaOH), producing Br^- and BrO_3^- . At pH=13.7 the green component corresponds to BrO^- . A third component is present at pH=9 (violet) and can be associated with HBrO . Interestingly, while the binding energy shift among the different anionic species correlates well with the increase of the oxidation state of bromine, the HBrO experimental point lays outside the correlation. The chemical shift is proportional to the screening effect experienced by the photoemitted electrons. Our results suggest that Br^- , BrO^- and BrO_3^- have a similar solvation environment, whereas HBrO differs. MD simulations helped us to contextualize the experimental results. HBrO is the only species displaying surface propensity, thus its solvation

environment is incomplete. The proposed complete in situ characterization may offer new insights about the reaction mechanisms at the liquid-gas interface.

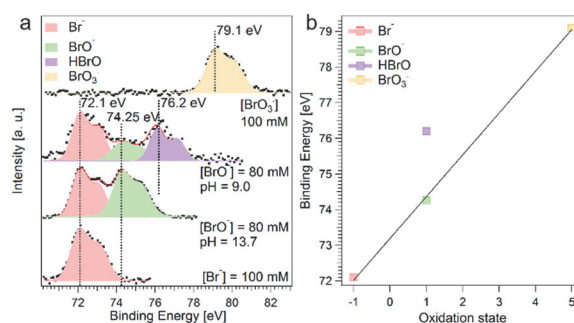


Fig. 1: (a) XPS of the Br 3d (KE=270 eV) core level peaks of 4 different solutions. The plot shows also the deconvolution of the peaks and their assignment. (b) Plot of the binding energy shift observed experimentally with the corresponding oxidation state of bromine.

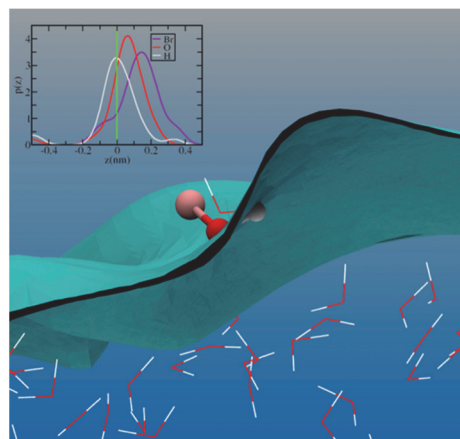


Fig. 2: Snapshot of HBrO molecule at the liquid-gas interface. In the inset the probability distribution of the location of each atom (white: H, red: O, pink: Br) in the HBrO molecule at the liquid-gas interface defined as Willard-Chandler dividing surface (green line).

- [1] W. R. Simpson et al., *Atmos. Chem. Phys.*, **7**, 4375 (2007).
- [2] L. A. Barrie et al., *Nature*, **334**, 138 (1988).
- [3] F. Domine, P. B. Shepson, *Science*, **297**, 1506 (2002).
- [4] L. Artiglia et al., *Nature Comm.*, **8**, 700 (2017).
- [5] M. Brown et al., *Rev. Sci. Instrum.*, **84**, 073904 (2013).

CATIONIC AND ANIONIC SURFACTANTS AFFECT SURFACE BROMIDE

S. Chen (PSI & ETHZ), L. Artiglia (PSI LSK & LUC), H. Yang (PSI & ETHZ), A. Boucly (PSI LEC & LUC), A. Laso, M. Ammann (PSI)

Oxidation of bromide has been found critical in initiating halogen-cycling reactions in marine air. Here, we report the chemical composition at the liquid-vapor interface of mixed aqueous solutions containing bromide and hexylammonium or propylsulfate as organic surfactants by liquid jet XPS.

Oxidation of bromide to hypobromite has been found critical in initiating halogen cycling reactions that later drive O_3 depleting chemistry in the troposphere [1]. The bromide reaction is enhanced at the aqueous solution-air interface [2]. The ubiquitous presence of organic compounds deriving from marine biota at the ocean surface calls for an assessment of the impact of often surface-active organics on the interfacial abundance of halide ions [3]. Here, we use liquid jet X-ray photoelectron spectroscopy (XPS) at the Swiss Light Source (SLS) [4] to assess the difference between a monofunctional surfactant with a positive headgroup (hexylammonium) and a negative headgroup (propylsulfate) on the abundance of bromide ions at the interface within the probe depth of XPS.

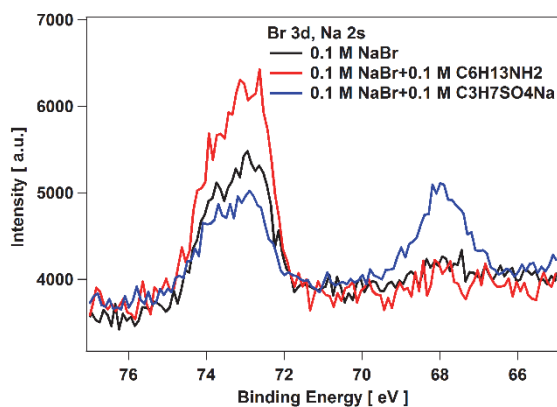


Fig. 1: Br 3d and Na 2s spectra of 0.1 M NaBr, mixed 0.1 M hexylammonium and 0.1 M NaBr, and mixed 0.1 M sodium propylsulfate and 0.1 M NaBr aqueous solutions at a kinetic energy of 155 eV.

Fig. 1 shows combined Br 3d and Na 2s photoelectron spectra of 0.1 M NaBr, mixed 0.1 M hexylammonium and 0.1 M NaBr, and mixed 0.1 M sodium propylsulfate and 0.1 M NaBr aqueous solutions at a kinetic energy of 155 eV. The Br 3d spectra consist of spin-orbit split doublets. Upon adding 0.1 M hexylammonium, the Br 3d peaks increase by 50% in comparison to pure NaBr solutions. The increased bromide intensity indicates that the positively charged ammonium headgroup in the hexylamine solutions (pH = 8.18) attracts more bromide towards the interface. This may be related to the electrostatic attraction between cation and anion for hexylammonium and bromide. In contrast, upon adding 0.1 M propylsulfate, the bromide intensity decreases by

30%. The decreased bromide intensity can be explained by the negatively charged headgroup of propylsulfate repelling bromide more into the bulk. And the increased sodium intensity is due to the anionic surfactant attracting more sodium cations into the interface.

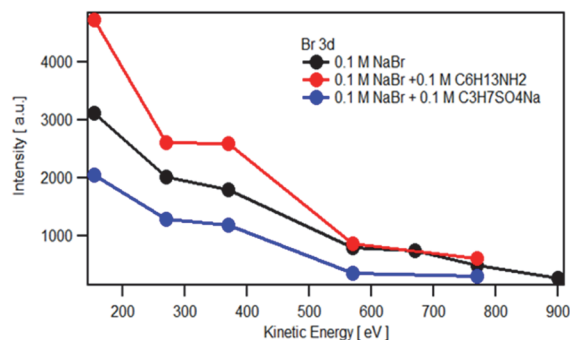


Fig. 2: Br 3d signal intensity of 0.1 M NaBr, mixed 0.1 M hexylammonium and 0.1 M NaBr, and mixed 0.1 M sodium propylsulfate and 0.1 M NaBr aqueous solutions as a function of electron kinetic energy.

In addition, we acquired Br 3d core level spectra as a function of kinetic energy for the same three solutions. The intensity of bromide decreases as a function of kinetic energy, which is related to the surface propensity of bromide, the photon flux, cross section and transmission function. The surface propensity of bromide on neat NaBr has been debated recently, but it seems that its concentration is not enhanced as previously suggested [5]. Therefore, the decrease is predominantly due to the other factors mentioned. In presence of hexylammonium and propylsulfate, the Br signal intensity is higher and lower, respectively, compared to pure NaBr at all kinetic energies, similar to those shown in Fig. 1. Further analysis of the kinetic energy dependence, also considering the attenuation effects by the aliphatic surfactant chains, can be used to quantitatively assess the surface concentration of bromide for the two differently charged surfactants.

We acknowledge funding from the Swiss National Science Foundation (Grant 169176).

- [1] S. Wang et al., Proc. Natl. Acad. Sci., **112**, 9281-9286 (2015).
- [2] L. Artiglia et al., Nature Comm., **8**, 700 (2017).
- [3] M. T. Lee et al., Phys. Chem. Chem. Phys., **21**, 8418 (2019).
- [4] M. A. Brown et al., Rev. Sci. Instrum, **84**, 073904 (2013).
- [5] M. T. Lee et al., J. Phys. Chem. A., **119**, 4600 (2015).

A CATIONIC SURFACTANT ACCELERATES BROMIDE OXIDATION

S. Chen, J. Edebeli (PSI & ETHZ), M. Ammann (PSI)

The reaction of ozone with sea-salt derived bromide is relevant for marine boundary layer chemistry. This study shows an obvious enhancement of ozone uptake to bromide solutions in presence of a cationic alkylammonium surfactant.

The multiphase reaction of bromide with ozone is an important bromide oxidation pathway, which later drives ozone depleting chemistry in the gas phase of marine air masses. The reaction exhibits an enhanced rate at the surface [1]. The ocean surface water and sea spray aerosol contain organic compounds, which may have a significant effect on the distribution of halide ions at the interface [2]. We selected tetrabutylammonium (TBA) for this study as a proxy for cationic surfactants deriving from biogenic oceanic material.

Solutions composed of 0.1 M TBA bromide (TBA-Br) / 0.55 M NaCl, 0.1 M TBA-Br only, 0.1 M NaBr / 0.55 M NaCl, and 0.1 M NaBr only, were used, respectively. TBA is expected to exhibit a surface excess of around 2.3×10^{14} molecule per cm^2 at 0.1 M [3]. The uptake coefficient of O_3 (γ_{obs}) is derived from the observed fractional loss of O_3 over a trough containing the aforementioned solutions and housed in a temperature-controlled reactor. In equ. 1, ω_{O_3} is the mean thermal velocity of the O_3 molecules in the gas phase (cm s^{-1}), $[\text{O}_3, \text{bypass}]$ is the measured O_3 concentration delivered to the reactor. $[\text{O}_3, \text{reactor}]$ is the O_3 concentration downstream of the reactor. Q is the flow rate of the gas passing through the reactor ($\text{cm}^3 \text{s}^{-1}$). SA is the total surface area of the solution (cm^2).

$$\gamma_{\text{obs}} = \frac{4 \cdot Q}{\omega_{\text{O}_3} \cdot SA_{\text{reactor}}} \times \ln\left(\frac{[\text{O}_3, \text{bypass}]}{[\text{O}_3, \text{reactor}]}\right) \quad (1)$$

Fig. 1 shows the measured O_3 uptake coefficients at 277 K as a function of O_3 concentration in the gas phase. Lines are fits with a kinetic model consisting of a combination of a surface reaction and a reaction-diffusion mechanism in the bulk [1]. At high O_3 concentration (above 200 ppb), γ_{obs} is constant, whereas at low atmospherically relevant O_3 concentration (between 30 and 100 ppb), γ_{obs} is decreasing. In previous studies [1,4], this behaviour has been attributed to a surface reaction dominating at low O_3 concentration. It results from the fact that the maximum coverage of O_3 on the surface is limited, which leads to the surface reaction rate saturating with higher O_3 concentration. This is not the case for the bulk phase reaction, since the bulk phase concentration of O_3 scales linearly with the gas phase concentration (Henry's law) in the relevant concentration range. The behaviour of the uptake coefficient shown in Fig. 1 is the result of the combination of parallel reaction in the bulk and reaction on the surface. The measured γ_{obs} in absence of TBA are consistent with previous studies from our group [1] and the work

by Oldridge and Abbatt [4]. The difference between the pure NaBr and the mixed NaBr/NaCl solutions may be explained by the lower solubility of O_3 due to salting out by NaCl. In presence of TBA, the O_3 uptake coefficient is higher than on the pure NaBr and NaBr/NaCl mixed solutions at low O_3 concentration, whereas they tend to be similar at high O_3 concentration. In presence of TBA, the effect of NaCl is not apparent at low O_3 concentration, which may be due to the fact that the concentration of the $[\text{Br} \cdot \text{OOO}]^-$ intermediate at the interface is independent of the presence of NaCl. However, at high O_3 concentration, a lower O_3 uptake coefficient was observed due to the salting out effect for the bulk reaction.

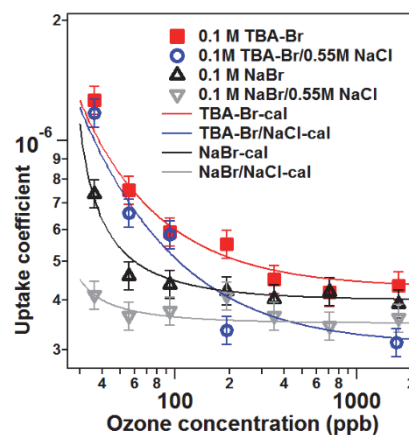


Fig. 1: Uptake coefficients of ozone as a function of ozone concentration in the gas phase.

It appears that the positively charged ammonium group in TBA helps to attract Br^- ions to the interface and possibly also leads to enhanced and saturated surface concentration of the $[\text{Br} \cdot \text{OOO}]^-$ intermediate that limits the reaction rate [1]. The salting out effect by NaCl is observed in the solution in presence of TBA. Further, such enhanced O_3 uptake on the surface is also in agreement with the liquid-jet XPS results.

We acknowledge funding from the Swiss National Science Foundation (Grant 169176).

- [1] L. Artiglia et al., *Nature Comm.*, **8**, 700 (2017).
- [2] M.-T. Lee et al., *J. Phys. Chem. A*, **119**, 4600-4608 (2015).
- [3] J. Mata et al., *Coll. Surf. A*, **245**, 69-73 (2004).
- [4] N. Oldridge et al., *J. Phys. Chem. A*, **115**, 2590-2598 (2011).

TEMPERATURE DEPENDENCE OF THE STRUCTURE OF LIQUID WATER

J. P. Gabathuler, H. Yang (PSI & ETHZ), A. Boucly (PSI LEC & LUC), L. Artiglia (PSI LSK & LUC), A. Laso, M. Ammann, T. Bartels-Rausch (PSI)

Liquid water, by definition of a liquid, has no fixed structure. Intermolecular bonds are constantly breaking and reforming. Here, we probe the local disorder of the hydrogen bonding network and show that the warmer the water, the more disordered it is.

Liquid water can be viewed as a jumble of water molecules interacting with each other by forming, breaking and reforming hydrogen bonds. While neutron scattering studies and computer simulation supports the idea that the water molecule is on average bonded to 4 other molecules in the constantly reorganizing hydrogen bonding network, more recent studies claim that the molecules binds on average to only 2 other molecules and that the structure of liquid water is made of chains and ring [1].

To learn more about the structure of liquid water, we take advantage of the near ambient pressure X-ray absorption (NEXAFS) spectroscopy technique to probe directly the structure of the hydrogen bonding network of liquid water as a function of temperature. Experiments were done with a liquid jet at the ISS beamline. Figure 1 shows the partial Auger-Meitner electron-yield NEXAFS spectra at the oxygen K-edge of liquid water at two temperatures. When detecting electrons, NEXAFS becomes inherently sensitive to the upper few nm of interfaces. The ‘warm’ water is at room temperature ($\sim 20^\circ\text{C}$) and the ‘cold’ water was cooled to 0°C by a jacket around the capillary delivering the liquid to the experiment. The spectra were acquired with a kinetic energy window of 412 to 437 eV. The background has been removed and the spectra are normalized to their integrated area between 527 and 560 eV. The upper plot shows the relative difference between the warm and the cold water together with a gas phase spectrum for comparison.

We see a small but notable difference in the two spectra in the regions denoted A, B, and C in Fig. 1. The relative difference i.e. $\frac{\text{Warm}-\text{Cold}}{\text{Warm}(540\text{eV})}$ [%] is plotted in the upper graph. Regions A and B show an increase in intensity with increasing temperature and region C a decrease in line with previous work [2]. Features A and B might be affected by the gas-phase peaks. The feature in region C can be assigned to a tetrahedral structure of the hydrogen-bonding network as also seen in ice [2]. This suggests that the colder the water, the more ordered the hydrogen bonding structure is. A stronger gas-phase signal intensity for the warm water sample makes sense since the warm water has a higher vapour pressure. Given that the diameter of the X-ray beam is larger than that of the liquid jet, gas phase surrounding the liquid jet, to which water molecules evaporate from the jet, is also probed.

If we assume that the liquid spectra at any temperature can be constructed from a linear combination of warm water and ice spectra, it would be very interesting to see if the ‘Liquid-like fraction’ follows the same trend as the bulk density i.e. with a maximum at 4°C . The increasing disorder with increasing temperature observed here for the air-water interface is in qualitative agreement with earlier NEXAFS spectroscopy work probing the interior of liquid water [2]. A detailed analysis to tackle differences in the temperature trend of the hydrogen bonding network structure between the surface and bulk of water is on-going.

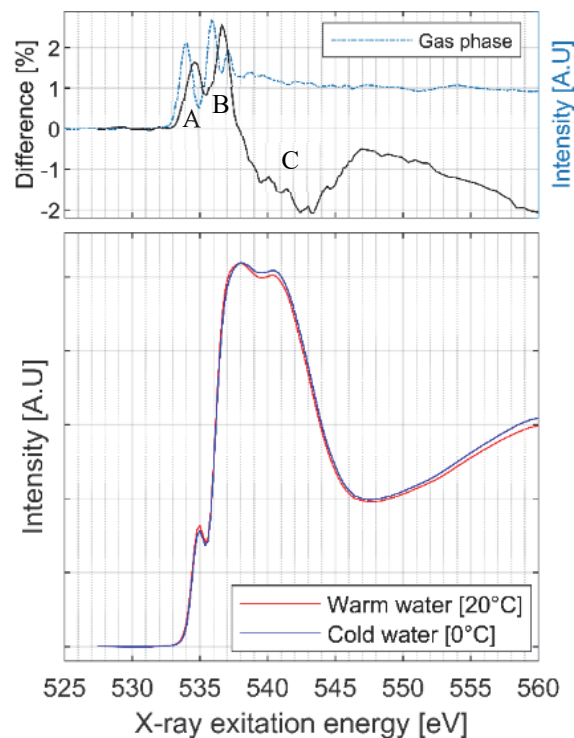


Fig. 1: Partial Auger-Meitner electron-yield NEXAFS spectra of liquid water at 0°C and 20°C . The liquid water data were acquired with the liquid jet experiment at the SIM beamline. The gas-phase data was acquired at the ISS beamline.

We acknowledge funding from the Swiss National Science Foundation (Grant 178 962).

- [1] P. Wernet et al., *Science*, **304**, 995-999 (2004).
- [2] A. Nilsson et al., *J. Electron. Spectros. Relat. Phenomena*, **177**, 99-129 (2010).

WATER ORGANISATION NEAR SURFACE ACTIVE ORGANICS

H. Yang (PSI & ETHZ), L. Artiglia (PSI LSK & LUC), J. P. Gabathuler (PSI & ETHZ), A. Boucly (PSI LEC & LUC), S. Chen (PSI & ETHZ), M. Ammann (PSI)

Surface-active organic solutes may induce a change to the hydrogen bonding (HB) structure in liquid water near the solution surface due to specific arrangements of hydrophilic functional groups. This is monitored by surface sensitive electron yield oxygen K-edge NEXAFS spectra of such solutions.

For aqueous solutions and ice, oxygen K-edge NEXAFS spectroscopy has been used extensively to probe the lowest unoccupied molecular orbitals of oxygen. They are controlled by the physical and chemical environment the water molecules experience, and hydrogen bonding (HB) between water molecules is a result of that. Ice and liquid water have a rather different hydrogen bonding (HB) network: in ice, water molecules are all tetrahedrally coordinated, which leads to a symmetrical HB network represented by a strong absorption peak above 540 eV in the NEXAFS spectrum (post edge). On the other hand, in liquid water, molecules are more disordered: weaker and asymmetric HB are represented by absorptions in the pre and main edge region, 535 – 538 eV [1, 2]. In this work, we use liquid water and ice as the two extreme cases for references of a given solution surface to characterize its HB network, which is a direct description of how water molecules are coordinated between themselves. Hence, increasing absorption at higher energy (post-edge) indicates relatively more ordered HB.

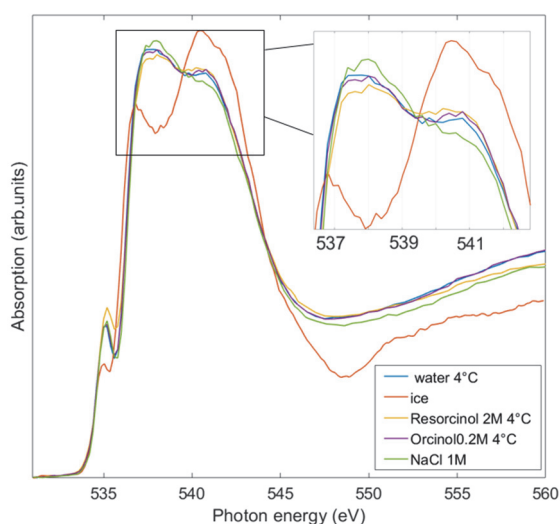


Fig. 1: O K edge electron yield NEXAFS spectra of liquid water (blue), ice (red), resorcinol 2M (yellow), orcinol 0.2M (purple) and NaCl 2M (green) solution. All spectra are background off-setted and normalized by their area.

We have measured the O K-edge NEXAFS spectra of 2M resorcinol (1,3-dihydroxybenzene) and 0.2 M orcinol (3,5-dihydroxytoluene) solutions. Hydroxy-substi-

tuted aromatic compounds are pyrolysis products of lignin polymers and therefore are components of biomass burning aerosol. They also occur as ring-retaining products of oxidation of benzene and toluene in the gas phase. Trihydroxybenzene (THB) has been demonstrated to be a very efficient ice nucleation agent when immersed in aqueous solution [3], and we have demonstrated in previous experiments that THB appears to have a significant effect on the HB structure at the surface of THB containing solutions. In this report, we have continued these investigations with the structurally similar compounds, resorcinol and orcinol.

In Fig. 1 we show the oxygen K edge NEXAFS spectra of the 2 M resorcinol (red) and 0.2 M orcinol solutions at 4 °C. Resorcinol and orcinol are surface active that leads to a high surface density due to the combination of hydrophilic OH groups with hydrophobic moieties. In comparison with liquid water (blue) and ice (purple) spectra, the resorcinol solution shows a decrease in the intensity of the main edge observed at around 537.5 eV with a concomitant increase in the postedge located at around 541eV. This result indicates that near the surface of the resorcinol solution, tetrahedrally coordinated water molecules (or stronger HB) are more abundant than in pure water. The orcinol solution exhibits a similar effect. In contrast, in an ionic salt solution the formation of tetrahedrally coordinated water structures is less favorable, which eventually makes the formation of ice more difficult. Therefore, in Fig. 1 we also show the O K edge NEXAFS spectrum of a 1M NaCl solution (green). Clearly, a higher main edge and a lower post edge absorption feature is observed, in accordance with Cappa et al. [4].

Apart from the NEXAFS spectra, the concentration of the surface active organic species at the solution surface was monitored by XPS. In combination with surface tension data, this will allow retrieving the surface excess of these species to complement the information about HB.

We acknowledge funding from the Swiss National Science Foundation (Grant 169176).

- [1] P. Wernet, et al., *Science*, **304**, 995-999 (2004).
- [2] S. Myneni et al., *J. Phys.: Cond. Matter*, **14**, L213 (2002).
- [3] N. Fukuta, *J. Atmos. Sci.*, **23**, 191-196 (1966).
- [4] C. D. Cappa et al., *J. Phys. Chem. B*, **109**, 7046-7052 (2005).

X-RAY SPECTROMICROSCOPIC INVESTIGATION OF ICE FORMING PARTICLES

P. A. Alpert (PSI), A. Boucly (PSI LEC & LUC), A. Laso, M. Ammann (PSI), C. Padeste (PSI LMN), S. Finizio, B. Watts (PSI LSC)

Atmospheric ice formation is induced by roughly one in one million particles. A new ice nucleation instrument mounted inside an X-ray microscope has been developed to physically and chemically characterize those single particles that do and do not nucleate ice.

Precipitation is mostly formed via the ice phase in mixed phase clouds, and ice in clouds is very relevant for Earth's climate. Ice nucleation is the first step in freezing. Freezing or prevention of freezing is common to everyday life, e.g. for food and drug storage, icing and de-icing, and other industrial applications. However, the ice nucleation process is not well understood, since it occurs on the size scale of clusters of molecules and time scales of molecular fluctuations.

A new instrument to observe when ice forms was built, utilizing X-ray microscopy and spectroscopy to probe the physical and chemical properties of ice nucleating particles with 35 nm spatial resolution. This is the first time ice nucleation has been measured in-situ in an X-ray microscope. The main technical challenge was temperature, and thus relative humidity control, while maintaining X-ray transparency. A sketch of our setup is shown in Fig. 1.

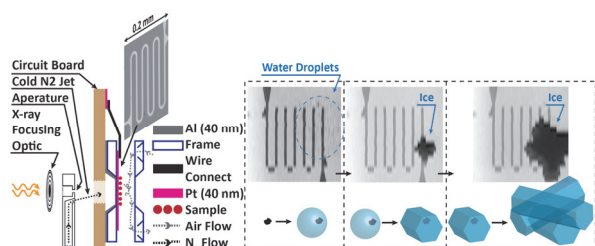


Fig. 1: Sketch of experimental setup is shown on the left (not to scale). The tilted optical microscope image of the Pt wire is shown. Three X-ray images on the right show water formation and the first instance of ice crystal formation followed by crystal growth.

In a standard configuration, X-rays are focused through an aperture onto our sample. We have modified the aperture to also host a jet of nitrogen and control its temperature down to 170 K. The cold jet is directed to the back of an environmental cell mounted on a circuit board. Inside the cell with front and back X-ray transparent windows (~ 100 nm thin), our sample is exposed to water vapor. The temperature of the sample is measured using a custom microfabricated sensor patterned using electron-beam lithography. Finally, the cold jet cools the sample only on the window exactly where we want ice nucleation to occur. An example of ice nucleation on iron containing nano-particles, ferrihydrite, is shown in Fig. 1. This iron mineral is contained in mineral dust, which itself is assumed to be ice active. We

can distinguish first, when water drops appear (blurred area), when ice first appears and grows, and measure the corresponding temperature and humidity.

Fig. 2 shows that the particle responsible for nucleating ice can be determined by sublimating ice. Close inspection reveals the particle is, in fact, ferrihydrite.

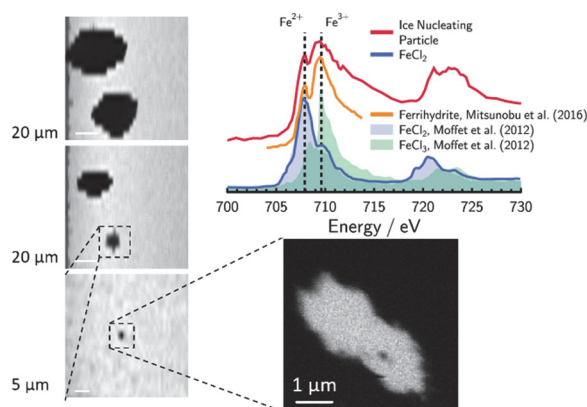


Fig. 2: In a sequence of four X-ray images shown above, nucleated ice crystals were sublimated slowly by keeping the ice saturation ratio slightly below 1.0. X-ray spectroscopy of the imaged ice nucleating particle was most similar to ferrihydrite as determined from literature [1] as opposed to other iron containing minerals such as iron chlorides, FeCl_2 and FeCl_3 , measured previously [2] and reproduced in this study.

This spot-cooling technique can be used for a wide range of applications and includes, in part, determining ice nucleating properties of natural aerosol samples or observing chemical changes due to reaction in aerosol particles at low temperature. As a user instrument at the PoLux endstation of the SLS, this will be available to researchers for a variety of disciplines.

We acknowledge funding from the European Union's Horizon 2020 research and innovation program under the Marie Skłodowska-Curie grant agreement (701647).

- [1] S. Mitsunobu et al., *Microbes Environ.*, **1**, 63-69 (2016).
- [2] R. Moffet et al., *J. Geophys. Res.*, **101**, D07204 (2012).

WATER ORGANISATION ON SILVER IODIDE SURFACES

H. Yang (PSI & ETHZ), L. Artiglia (PSI LSK & LUC), J. P. Gabathuler (PSI & ETHZ), A. Boucly (PSI LEC & LUC), S. Chen (PSI & ETHZ), M. Ammann (PSI)

Silver iodide particles are prominent ice nucleating particles (INP), as AgI promotes the formation of ice crystals in super cooled water. Hence, AgI is widely used for cloud seeding. This work aims at understanding the hydrogen bonding structure of adsorbed water on the surface of AgI particles in the context of deposition nucleation.

Water adsorption on a solid is the prerequisite for deposition nucleation, and the solid surface plays a crucial role in the nucleation process. The AgI surface is believed to be very ice nucleation active when exposed to water vapor [1]. Due to similar interactions between AgI and nearby water molecules, AgI in a cloud is able to induce freezing in liquid water at higher temperature ($-3\text{ }^{\circ}\text{C}$), while pure water droplets would freeze homogeneously below $-35\text{ }^{\circ}\text{C}$ [1]. In this work, electron yield near edge X-ray absorption fine structure (NEXAFS) spectroscopy at the oxygen K-edge is used to experimentally explore the hydrogen bonding structure of H_2O molecules adsorbed on AgI surfaces, under subsaturated humidity conditions with respect to ice. Experiments were performed at the *in situ* electron spectroscopy (ISS) beamline at the Swiss Light Source (PSI, SLS).

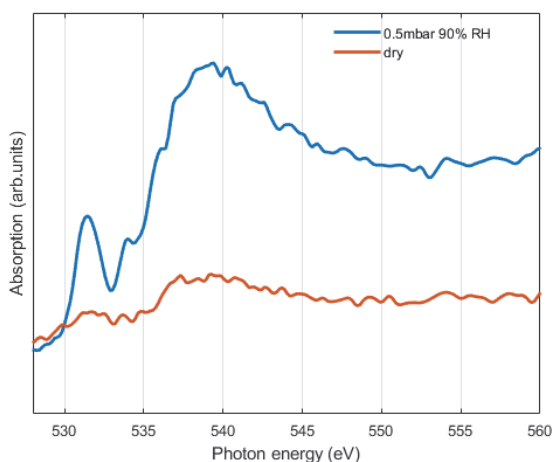


Fig. 1: Electron yield O K-edge NEXAFS spectra from AgI under dry conditions (red) and in presence of water vapour at 0.5 mbar at a relative humidity of 90 % at $-25\text{ }^{\circ}\text{C}$ (blue).

Our AgI particles were prepared by mixing 0.1 M KI and AgNO_3 in Milli-Q water. In Fig. 1 we show the electron yield O K-edge NEXAFS spectra from AgI under dry conditions, and at 90 % RH. The spectrum of the dry sample (Fig1, red) shows only little absorption at the oxygen edge possibly from some surface oxidation and oxidized adventitious carbon. On the other hand, when water vapor adsorbs on the sample surface at 90 % RH (Fig. 1, blue), a strong increase of absorption occurs starting from 538 eV due to the adsorbed

water. Also absorption at 532 eV increases, likely due to an increase or oxidation of organic contaminations.

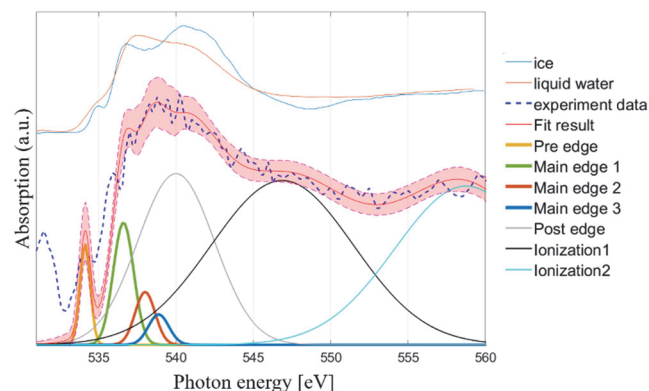


Fig. 2: The Gaussian deconvolution of the difference spectrum (dashed blue) of the two spectra shown in Fig. 1. Liquid water (thin red) and ice (thin blue) NEXAFS are also shown for comparison.

By subtracting the spectrum measured under dry conditions from that under humid conditions, we obtain the difference spectrum attributable to the adsorbed water (Fig. 2 dashed blue). This spectrum is fitted with 7 Gaussian peaks. The red shaded area represents the estimated error bounds with 95 % of confidence level. As references for the adsorbed water, the O K edge NEXAFS spectra of ice and liquid water are also shown in Fig.2. The absorption at 535eV and 538eV is strong in liquid water due to the weak or distorted H-bonds, while the tetrahedrally coordinated H-bond gives a strong absorption at 540-542eV in the ice spectrum [2]. The difference spectrum has rather higher absorption in the region above 540 eV (thick red, blue and grey peaks) than at 538 eV, which might indicate that under subsaturated conditions, the adsorbed water structure on AgI surfaces is already dominated by tetrahedrally coordinated water molecules to facilitate the formation of ice at just a little higher RH. This is in strong contrast to the behavior on TiO_2 particles recently studied [3].

We acknowledge funding from the Swiss National Science Foundation (Grant 169176).

- [1] Marcolli, C., et al., *Atmos. Chem. Phys.*, **16**(14) 2016.
- [2] Myneni, S., et al., *Journal of Physics: Condensed Matter*, **14**(8) 2002.
- [3] Orlando, F., et al., *Topics in Catalysis*, **59**(5) 2016.

MOLECULAR STRUCTURE OF WATER AT THE AIR-ICE INTERFACE

J. P. Gabathuler, H. Yang (PSI & ETHZ), A. Boucly (PSI LEC & LUC), L. Artiglia (PSI LSK & LUC), A. Laso, M. Ammann, T. Bartels-Rausch (PSI)

As temperature increases towards the melting point, disorder of the hydrogen-bonding network of ice at the interface with the gas phase increases, creating what we call the Quasi Liquid Layer (QLL). We take advantage of the surface-sensitivity of X-ray excited electron spectroscopy to shine light on this QLL.

Reports on the thickness of the QLL are ranging from 2 nm to 25 nm at 271 K for different probing techniques. Many processes have been suggested to depend directly on the QLL, ranging from the motion of glaciers to cloud electrification. While our goal is to understand the relevance for chemical processes in the atmosphere, the actual implications of the QLL are very broad, from molecular biology to material science.

Near Edge Absorption Fine Structure (NEXAFS) spectroscopy is an experimental technique to probe the energy states and hybridization of molecular orbitals and therefore, such measurements allow distinguishing water in its solid, liquid, and gas-phase state. If based on the detection of electrons, NEXAFS spectroscopy is highly sensitive to the surface region of a few nanometers [1].

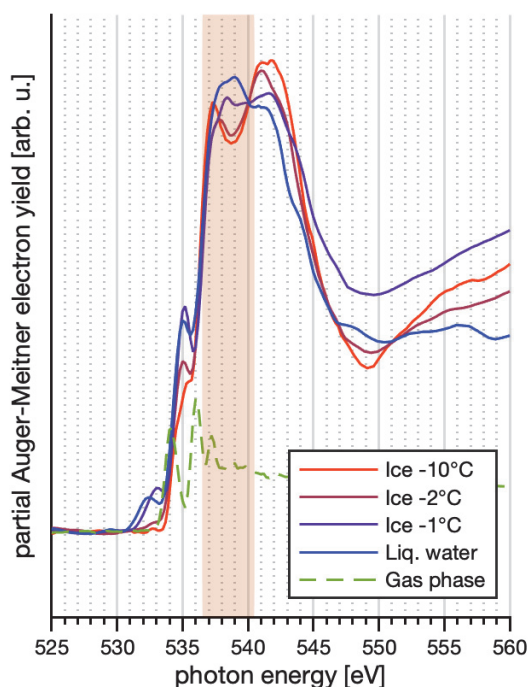


Fig. 1: O K-edge partial Auger-Meitner electron-yield NEXAFS spectra of ice at different temperature, liquid and gas-phase water.

Fig. 1 shows NEXAFS spectra of ice with increasing temperature acquired at the ISS beamline. NEXAFS spectra of liquid and gas-phase water acquired with the same experimental setup and measurement settings are also displayed for comparison. Looking at the region [536-540 eV] (Fig.1, orange rectangle), one can observe that the warm ice at -1 °C seems to be composed of approximately 50 % ‘cold ice’ and 50 % ‘liquid water’. The probing depth is about 2 nm or 6 crystal bilayers. Fig. 2 shows a compilation of the liquid fraction.

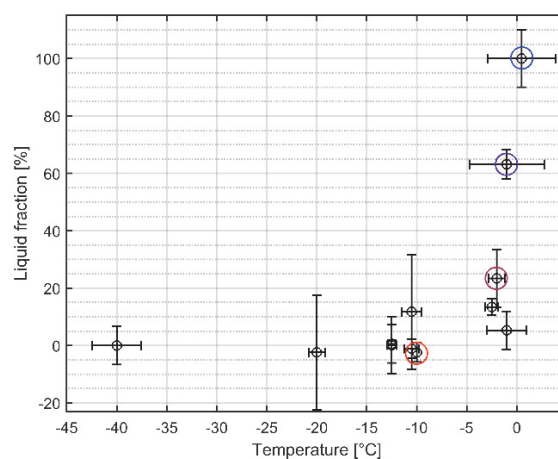


Fig. 2: Temperature dependence of the surface disorder of ice. The data points circled in color correspond to the NEXAFS spectra shown in Fig. 1.

The main conclusion of this preliminary data set is that the QLL is rather thin compared to other studies [2]. However, we cannot exclude that carbon contamination, which was higher during the measurement of warmer ice spectra, influenced the QLL thickness. The ongoing detailed analysis of the data will tackle this issue.

We acknowledge funding from the Swiss National Science Foundation SNF (grant 178 962).

- [1] M. Ammann et al., “X-Ray Excited Electron Spectroscopy to Study Gas–Liquid Interfaces of Atmospheric Relevance”, chapter in “Physical Chemistry of Gas-Liquid Interfaces” (J. A. Faust, J. E. House, eds.), Elsevier, p. 135-166, (2018).
- [2] T. Bartels-Rausch et al., *Atmos. Chem. Phys.*, **14**, 1587-1633 (2014).

HOW TO KEEP NITRATE STABLE UNDER AN X-RAY BEAM

Y. Manoharan, J. P. Gabathuler, H. Yang (PSI & ETHZ), A. Boucly (PSI LEC & LUC), L. Artiglia (PSI LSK & LUC), M. Ammann, T. Bartels-Rausch (PSI)

X-ray excited electron spectroscopy is a powerful tool to investigate environmental interfaces. However, the experiments can be destructive to the sample. Here, we describe how an optimized measurement strategy improves sample stability in experiments with sodium nitrate.

Photolysis of nitric acid (HNO_3) in polar snowpack releases nitrous acid (HONO) and nitrogen oxides ($\text{NO}_x = \text{NO} + \text{NO}_2$) to the atmosphere. Secondary reactions can then lead to the formation of nitrous acid (HONO). The emissions effect the budget of oxidants such as hydrogen oxide radicals and ozone in the troposphere. To obtain insight into the photochemical reactions of HNO_3 at the air-ice interface, X-ray excited electron spectroscopy will be used. Here, we report on first experiments at the SLS/ISS beamline.

In a first step, we optimized the stability of sodium nitrate (NaNO_3) during the recording of an X-ray photoemission spectrum (XPS). Nitrate has been found to be decomposed by X-rays and by secondary electrons both of which are present during XPS experiments [1].

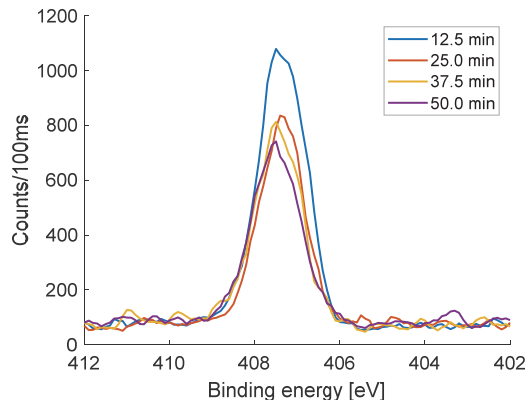


Fig. 1: N1s XPS spectra of a NaNO_3 sample with time measured with an excitation energy of 1000 eV at the SLS/ISS beamline. We performed this experiment under humid conditions with a partial pressure of water of approx. 1 mbar to reduce charging effects. The sample was at room temperature. Under these conditions the sodium nitrate is solid.

Fig. 1 shows that the XPS signal intensity stabilizes after 12 minutes. This was achieved by reducing the photon flux and it makes experiments over longer time-scales feasible. During this experiment, no increase of other species at the sample surface, such as adsorbed water or carbon species, was observed showing that stable experimental conditions were achieved.

Since our goal is to work with environmentally relevant concentrations of HNO_3 adsorbed on ice, the minimum

amount of nitrate on ice that gives a clear N1s XPS signal was estimated in the following. Figure 2 shows a typical O1s XPS spectrum of ice. Compared to the N1s in Fig. 1, the intensity is about five times higher, because oxygen has a higher absorption cross-section than nitrogen and is thus more sensitively detected. Furthermore, the amount of oxygen being probed in an ice sample is significantly higher than the amount of nitrogen probed in a nitrate salt sample, which has only one nitrogen atom per three oxygen atoms. Also shown in Fig. 2 is an estimated N1s signal for $4\text{E}14 \pm 8\text{E}13$ HNO_3 molecules/ cm^2 , which is 1.5 ± 0.3 monolayer of HNO_3 adsorbed on ice. Gas-phase-calibration measurements were used to estimate the N1s peak area relative to that of O1s. For this, we used a probing depth of 2.0 nm and assumed an O-O distance of 3 Å for the dense packing in ice.

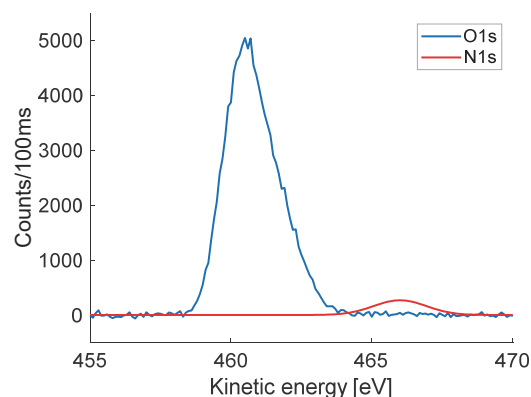


Fig. 2: O1s XPS spectrum of ice (blue line) at 1000 eV excitation energy. Also shown is the signal intensity that $4\text{E}14 \pm 8\text{E}13$ molecules nitrate per cm^2 would give.

These results show that nitrate at the air-ice interface can be investigated using X-ray excited electron spectroscopy at the SLS/ISS beamline with sufficient sensitivity and long-term stability.

We acknowledge funding from the Swiss National Science Foundation (Grant 178 962).

- [1] S. Aduru et al., J. Phys. Chem., **90**, 1683-1688 (1986).

WHAT DOES SNOW METAMORPHISM DO TO ITS CHEMICAL COMPONENTS?

S. E. Avak (PSI & Univ. Bern), T. Bartels-Rausch (PSI), J. Edebeli (PSI & ETHZ), A. Eichler (PSI), M. Schneebeli (WSL-SLF), J. C. Trachsel (WSL-SLF & ETHZ)

This question was central to the collaborative Miso project over the last four years. While being motivated by academic curiosity, answers are highly relevant to interpreting the chemical signals in ice cores as paleo-archives and for understanding current atmospheric chemistry in snow-covered regions.

Earth's snow cover is a multi-phase structure that holds chemical species in various compartments (Fig. 1) [1]. In their early work, Eichler et al., discussed how the specific location of impurities impacts their preservation in alpine firn proposing that some ions replace oxygen in the ice lattice and that these embedded ions are less easily washed away by meltwater than those located at the air-ice interface [2]. Taken that surface snow completely re-crystallizes every few days during metamorphism [3], the question arises how impurities in snow respond to the underlying water vapor fluxes and whether metamorphism leads to changes in their location.

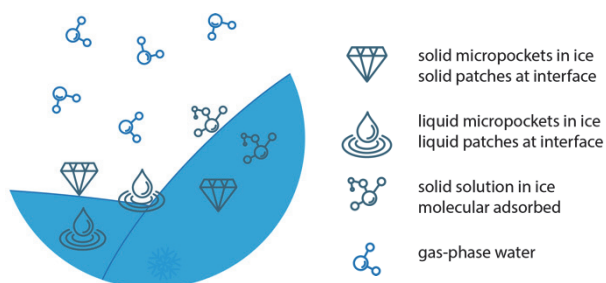


Fig. 1: Illustration of the compartments that can host chemical species in snow and environmental ice. Impurities can form solid (diamonds) and liquid (droplets) deposits at the air-ice interface and embedded within the snow interior, molecularly (molecule) adsorb at the interface, or embedded in the ice forming a solid solution.

Within the Miso project, Trachsel et al., showed substantial re-arrangement of ions with progressing metamorphism (Fig. 2) [4]. In particular, the changes were significant larger over 3 months of metamorphism when the snow was exposed to a temperature gradient. Temperature gradients are frequently observed in environmental snowpacks. The redistribution was found to be strongly dependent on the specific chemical compound. Calcium, sulfate, and sodium got enriched at the air-ice interface; ammonium, fluoride, and chloride buried in the interior of the snow.

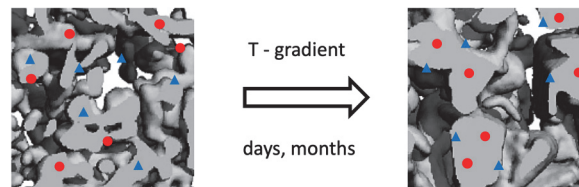


Fig. 2: Illustration of selective redistribution of ions in snow to the air-ice interface (blue triangles) or to the interior of the ice (red dots) with temperature gradient metamorphism.

This finding has direct consequences for interpreting ice core records to derive past atmospheric composition. Avak et al., linked the enrichment of ions at the air-ice interface with their enhanced mobilization by meltwater [5]. Once melt events occur, which is nowadays more frequently observed with climate warming, originally deposited impurities may be delocalized in ice cores. Avak et al., showed that chemical species such as ammonium and rare earth metals at low concentration are well preserved in snow in line with their burial in the ice matrix [5].

The location of chemical species in snow is also of importance for present-day atmospheric chemistry. Edebeli et al. showed that the heterogeneous oxidation of bromide in snow by gas-phase ozone ceases during 12 days of temperature gradient metamorphism [6]. This is one of the reactions that kicks off ozone depletion events in Polar areas. The burial of bromide during metamorphism might, at least partially, explain why field studies have observed large variations in the chemical activity of snow in different areas and of different age.

Concluding, the Miso project has linked the location of chemical species in snow to metamorphism and shown strong consequences on chemical reactivity and post-depositional mobilization in snow and glacier ice.

We acknowledge funding from the Swiss National Science Foundation (Grant 155 999).

- [1] T. Bartels-Rausch et al., *Atmos. Chem. Phys.*, **14**, 1587-1633 (2014).
- [2] A. Eichler et al., *Tellus B*, **53**, 192-203 (2001).
- [3] B. R. Pinzer et al., *Geophys. Res. Lett.*, **36**, L23503 (2009).
- [4] J. C. Trachsel et al., *Front. Earth Sci.*, **7**, 194 (2019).
- [5] S. E. Avak et al., *J. Geophys. Res.-Earth*, **124**, 1647-1657 (2019).
- [6] J. Edebeli, *Atmos. Chem. Phys.*, submitted (2020).

MAJOR IONS AND TRACE ELEMENTS IN SNOW FROM NORTHEASTERN CHINA

H. Xue (JLJU & PSI)

We sampled fresh seasonal snow across northeastern China from winter 2017 to spring 2018 and analyzed the concentration of major ions and trace elements to derive the composition of snow.

Snow is an important type of wet deposition; it can scavenge species from the atmosphere. From this point of view, snow is considered an ideal matrix to observe deposition from the atmosphere due to natural and anthropogenic activities. Recent environmental studies have been devoted to analyze snow in order to establish the concentration and composition profile of major ions and trace elements. The essential minerals and salts present in the snow can be used to assess the level of environmental pollution.

So far, a great deal of attention has been focused on snow characterization in the Polar, high latitudes, and high-altitude areas. However, studies on the composition and properties of chemicals in seasonal snow are limited. Northeastern China is one of the three largest seasonal snow-covered areas in China. Until now, only few investigations have been done in northeastern China. However, the air pollution there is massive due to input from anthropogenic activities, such as industrial manufacturing and coal combustion in winter. To attain a better understanding of the level of major ions and trace elements in cities and their sources in seasonal snow, a total of 60 snow samples from 16 sites across northeastern China were collected from December 2017 to March 2018. Major water-soluble ions (Cl^- , NO_3^- , SO_4^{2-} , Na^+ , NH_4^+ , K^+ , Ca^{2+} , Mg^{2+}) and trace elements (Mn, Cr, Cd, Ni, Cu, Zn, Pb, As, Fe) were analyzed.

The composition of ions and elements in snow is shown in Figure 1. The results indicate that Ca^{2+} and SO_4^{2-} are the major ions contributing up to 34 % and 23 % of major ions, respectively; Pb was the dominant element contributing up to 63 % of trace elements. Anthropogenic inputs, such as mining and smelting, coal combustion, and traffic emission made an important contribution. Compared with previous studies in northeastern China and other locations, both major ions and trace elements were found at relative high levels, especially Pb, and are therefore posing a threat to human health.

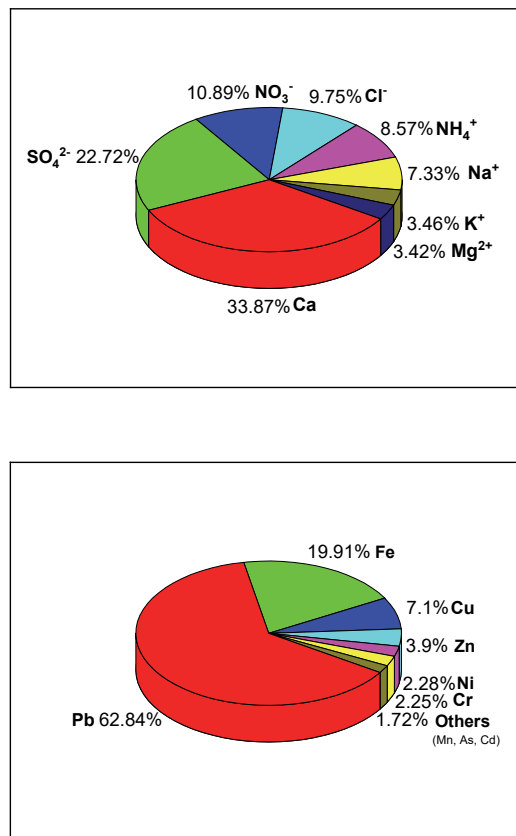


Fig. 1: Composition of major ions and trace elements in snow across northeastern China, 2017-2018

We acknowledge funding from the National Natural Science Foundation of China (41403101).

- [1] Z. Du, et al. *Sci. Total Environ.*, **675**, 380-389 (2019).
- [2] X. Wang, et al, *Atmos. Environ.*, **114**, 57-65 (2015).

ALTERING OF THE STABLE ISOTOPE SIGNAL IN AN ALPINE SNOW PACK

J. C. Trachsel (WSL-SLF & ETHZ), F. Aemisegger (ETHZ), A. Eichler, S. Brütsch, T. Bartels-Rausch (PSI), S. E. Avak (PSI & Univ. Bern), J. Edebeli (PSI & ETHZ), M. Schneebeli (WSL-SLF)

This study used water stable isotope measurements in a series of snowpit samples to investigate, how the deposited atmospheric isotope signal is altered in an Alpine snow pack.

Water stable isotope signals ($\delta^{18}\text{O}$, δD) in ice cores can be used for reconstructing past temperatures, since they depend on atmospheric (condensation) temperatures during precipitation formation. The isotopic signal deposited in snow is a complex function of cloud formation, atmospheric transport, precipitation and post depositional effects such as snow metamorphism, melting, and sublimation at the snow surface. However, in alpine snow these effects have not been investigated in detail. Here we present a series of five snow pit water stable isotope profiles taken at the Weissfluhjoch site (2536 m.a.s.l.) above Davos, Switzerland (Fig 1). The field campaign took place between January and June 2017. The five snowpits were sampled with a vertical resolution of 6 cm. In parallel, a four-month continuous gaseous water vapor measurement was performed at the same site.



Fig. 1: Left) Field site Weissfluhjoch in the Swiss Alps, 2536 m a.s.l. with a heated hut containing a Picarro analyzer and an inlet on the left side of the roof. Right) Sampling team in clean overalls and masks inside the snow pit to prevent contamination of the samples.

The five snowpits collected from January to June allowed to follow the development in the snowpack. The comparison revealed that during the cold season (samplings in January, February and March) the isotopic records agree well [1] (Fig. 2). There was a slight smoothing observed at a scale of about 10 cm, that is most probably the result of dry snow metamorphism.

On 17 April partial melting occurred and the recorded profile shows a clear smoothing. As soon as rain- or meltwater is present in the snow cover, a complex system of recrystallization, mixing, and fractionation processes is established [2].

On the last sampling day on 1 June the total snow profile was isothermal and soaked with meltwater. The formation of meltwater resulted in a significant shift of the original isotopic signal towards higher $\delta^{18}\text{O}$ values in the snowpack of up to several permille. However, despite this clear overall enrichment in the snowpack, the $\delta^{18}\text{O}$ variability is still preserved to some extent with a preservation of the local maxima and minima (Fig 2).

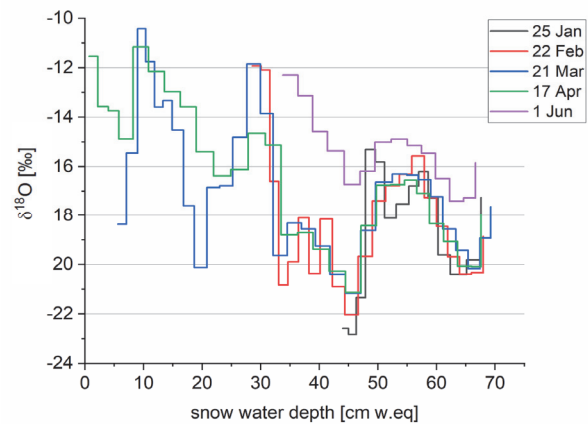


Fig. 2: Records of $\delta^{18}\text{O}$ in five snow pits at Weissfluhjoch above Davos in winter 2016/2017. The ground surface is at 67 cm w. eq. and the surface of the snow cover at different snow water depths depending on the snow cover extent. The first three snow pits, 25 Jan 2017 (black), 22 Feb 2017 (red) and 21 Mar 2017 (blue), were taken in cold conditions, 17 Apr 2017 (green) was isothermal and partial melted, during the last one on 01 June 2017 (violet) the snowpack was wet and percolating meltwater was observed.

Further, the signals of isotopes, which were deposited in the snow cover, could be assigned to individual precipitation events and associated with precipitation from cold or warm air masses by the application of weather models and the modeled density development from the snow cover model SNOWPACK [3]. The isotopic composition reflects the passage of warm fronts (increasing $\delta^{18}\text{O}$ and maxima at 10, 30, and 50 cm w.eq.) and cold fronts (drops in $\delta^{18}\text{O}$ and minima at 20, 45, and 65 cm w.eq.). Thus, our results indicate that the isotopic signature of the snowpack provides a record of the weather pattern throughout the winter season, but only as long as there is no meltwater percolation.

The detailed influence of frontal systems on the isotope records in the snow pack and the continuous water vapor measurements will be investigated in more detail in a follow-up study.

We acknowledge funding from the Swiss National Science Foundation (Grant 155 999).

<https://www.psi.ch/luc/miso>

- [1] J. C. Trachsel, Dissertation, ETHZ research-collection (2019).
- [2] S. Taylor et al., *Water Res. Res.* **37**, 759-769 (2001).
- [3] P. Bartelt and M. Lehning, *Cold Reg. Sci. Technol.* **35**, 123-145 (2002).

SNOW ACCUMULATION STUDIES IN THE CENTRAL KARAKORAM

A. R. Groos (Univ. Bern), S. Erlwein (TUM), C. Mayer, A. Lambrecht (BAdW), S. Brüttsch, A. Eichler (PSI), M. Schwikowski (PSI & Univ. Bern)

The Karakoram in the northwestern part of High Mountain Asia has increasingly attracted attention due to an anomalous glacier stability, which contrasts elsewhere observed progressing ice mass loss. We used snow samples from high elevation accumulation sites for water stable isotope analysis to investigate recent spatio-temporal precipitation variations in the Central Karakoram.

Increasing winter precipitation is discussed as a potential cause for the Karakoram anomaly. However, the lack of high-altitude weather stations and glaciological measurements hampers the corroboration of this hypothesis. In 1986, Canadian researchers conducted high elevation snow accumulation studies at the Biafo-Hispar glacier-system in Central Karakoram [1,2]. During our field expedition in June/July 2019, we revisited their study sites and excavated eight snow pits between 4,388 and 5,202 m (Fig.1).



Fig. 1: Excavation of snow pits during the field survey at Biafo-Hispar glacier system in June/July 2019.

Density measurements were performed in 20 cm intervals to detect individual precipitation events and quantify elevation-dependent annual snow accumulation. At three selected pits, snow samples were retrieved in 10 cm intervals for the analysis of water stable isotopes ($\delta^{18}\text{O}$ and $\delta^2\text{H}$) and the elemental composition of detected dust events. For more than 170 samples, $\delta^{18}\text{O}$ and $\delta^2\text{H}$ were analysed at the Paul Scherrer Institute.

Our first results indicate a pronounced increase of annual snow accumulation with elevation. The respective snow water equivalent vary between <500 and $>2,000$ mm. Prominent density peaks in 4 m respectively 5 m depth relate to occurrence of thick ice lenses hinting towards summer melt layers. The relative relationship between $\delta^{18}\text{O}$ values and air temperatures – low $\delta^{18}\text{O}$ values indicate low atmospheric temperatures during water condensation – confirm this assumption (Fig. 2).

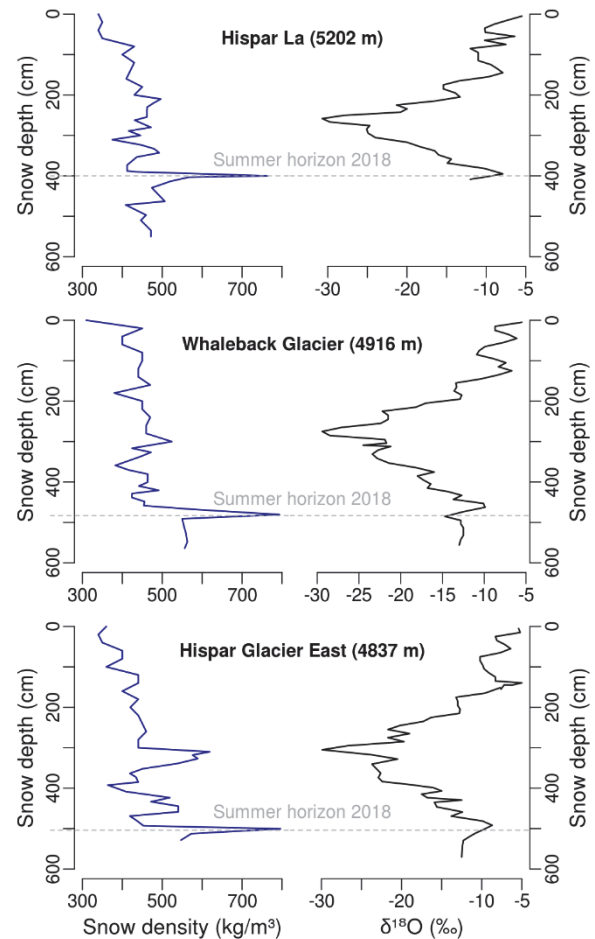


Fig. 2: Snow density and $\delta^{18}\text{O}$ of three snow pits from the Biafo-Hispar system.

The well-preserved structure and isotope signature of snowfall events in the investigated snow pits demonstrate that the high elevation accumulation basins in the Karakoram are a valuable archive for reconstructing precipitation variations in the region. In a next step, the elemental composition of detected dust layers will be analysed to trace the origin of individual snow fall events. In addition, snow density and ^{18}O records will be linked to weather station data to quantify the amount of winter and summer accumulation.

We acknowledge funding from the National Geographic Society (Early Career Grant), the University of Bern (Open Round 2019) and the Bavarian Academy of Sciences.

- [1] K. Hewitt, et al., *A. Glaciol.*, **13**, 103-108 (1989).
 [2] C. P. Wake, *A. Glaciol.* **13**, 279-284 (1989).

SIMILAR FIRN CHARACTERISTICS AFTER 5 DECADES ON ABRAMOV GLACIER

M. Kronenberg (Univ. Fribourg), A. Eichler, S. Brütsch (PSI), M. Schwikowski (PSI & Univ. Bern), M. Hoelzle, H. Machguth (Univ. Fribourg)

A recent firn core from a historical firn investigation site and complementary data including Ground Penetrating Radar (GPR) measurements allow for a reassessment of firn conditions after 5 decades on Abramov Glacier, Pamir Alay. Results indicate overall similar firn conditions and accumulation rates compared to the 1970s.

The firn cover of mountain glaciers is expected to undergo changes related to global warming. For Abramov glacier, located in the Pamir Alay in southern Kyrgyzstan, firn profiles from the 1970s are available [1]. The glacier is temperate and covers an elevation range of ~3800-5000 m a.s.l. The main firn investigation site was located in the orographic right accumulation area at 4410 m a.s.l. According to a firn profile from June 1973, average accumulation rates for the period 1965-72 were 0.7 ± 0.5 m w.e. yr⁻¹. In the 1970s, the firn profile was characterised by the abundance of ice layers. Furthermore, during the melt period, a firn aquifer was observed at a depth of about 10 m.

Here we investigate the current firn characteristics of Abramov glacier and compare them to these legacy measurements of the 1970s. Our approach consists in spatially connecting accumulation rates determined for a well-dated 17 m firn core drilled at 4392 m a.s.l. in February 2018 (*core_4392*, [2]) to the site of historical investigations. The drill site of the *core_4392* is in close vicinity of the (originally unknown) location of the studies of the 1970s. A GPR profile, measured with an 800 MHz shielded antenna during the drilling campaign, revealed that net accumulation rates around the drill site vary strongly. Hence, a direct comparison of new and historic data necessitated finding the precise location of the historic drill sites. We assessed a manifold set of information to determine the exact location and eventually drilled an additional firn core (*core_4395*).

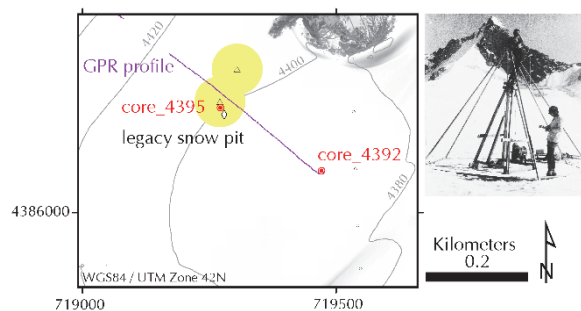


Fig. 1: Left: Location map of *cores_4392* and *4395* (red), GPR Profile (purple), and transformed coordinates (white). Yellow circles indicate 50 m uncertainty of the location of the photographer of the legacy pictures. Right: Example picture of core drilling in the 1970s (unknown photographer).

Benchmark coordinates recorded with a differential GPS and information from past investigators allowed for coordinate transformation and identification of the exact location of the legacy firn profiles (reported in a local coordinate system). The site was situated about 250 m from the location of the dated *core_4392*. Legacy photographs allowed us to validate the location determined with the coordinate transformation (Fig. 1). Our GPR data indicated lower accumulation rates for the historical drill site. Therefore, we drilled an additional core in August 2018. *Core_4395*, was analysed for stratigraphy and density. We furthermore performed extensive GPR measurements for a better understanding of the spatial accumulation heterogeneity.

The accumulation rates of *core_4395* were extracted from *core_4392* based on dust layers visible in both cores and GPR data (Fig.2). In *core_4395*, the summer horizon 2011 corresponds to a depth of 9.5 m. Annual accumulation rates 2011-18 are 0.84 ± 0.24 m w.e.yr⁻¹.

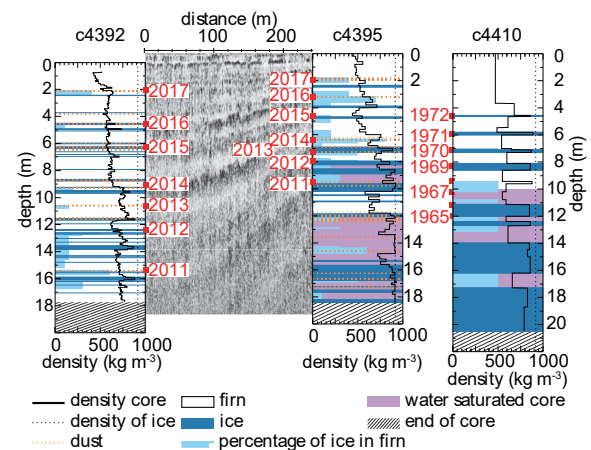


Fig. 2: Firn stratigraphy of dated *core_4392*, spatial extraction of annual horizons with GPR to *core_4395*. Legacy core 4410 is plotted for comparison.

Recent accumulation rates 2011-18 are comparable to those of the period 1965-72 within the range of inter-annual variability. The visible firn stratigraphy remains similar for both cores (Fig. 2). The fraction of continuous ice layers is reduced (21 % compared to 30 % in the 1970s), whereas, firn layers have a higher variable ice content in 2018. The average density is higher for the recent core (720 vs. 650 kg m⁻³).

Overall, these results indicate relatively stable firn conditions at an elevation of 4400 m a.s.l. on Abramov glacier.

We acknowledge funding from the Swiss National Science Foundation (Grant 200021_169453).

[1] B. V. Kislov. SARNIGMI Tashkent (1982).

[2] M. Kronenberg, Annual Report LUC 2018, p. 30.

LIGHT ABSORBING IMPURITIES IN THE OLIVARES BASIN, CENTRAL CHILE

M. Barandun (PSI & Univ. Fribourg), A. Rivera (CECs), B. Grobety (Univ. Fribourg), L. Fang, S. Köchli (PSI), K. Naegeli (Univ. Bern), M. Schwikowski (PSI & Univ. Bern)

Light absorbing impurities can lower glacier albedo considerably. The glacier darkening enhances glacier melt. Here, we investigate the source and role of impurities at the glacier surface for the Olivares basin, Central Chile.

The Andes, with a mean annual glacier mass balance of -0.72 ± 0.22 m w.e. yr⁻¹ for 2000–2018, is one of the regions with highest mass loss worldwide [1]. In the future, glacier retreat is expected to intensify. Due to glacier mass loss, the Andes will lose 30 % of meltwater contribution to total river runoff in the next 100 years [2]. This will have major consequences for the fresh water availability of the region. High anthropogenic light absorbing impurity (LAI) content in snow of Central Chile include not only elevated concentrations of elemental carbon but also of mineral dust [3]. For the Olivares basin the sources of LAIs, their role on glacier-wide albedo and the associated magnitude of ablation are so far not well understood. This study aims to (1) characterize LAIs detected in snow and ice, (2) quantify albedo based on *in situ* measurements and satellite imagery, and (3) estimate the effect on the ablation processes of the Olivares glaciers.

Ice surface and snow samples of 2018 and 2019 from glacier Olivares Alfa (OA), Beta (OB), Paloma Norte (PN) and Juncal Sur (JS) were analyzed for organic (OC) and elemental carbon (EC) using a thermal-optical method. We used inductively coupled plasma optical emission spectrometry to detect trace element concentrations. Comparing this to a natural background from Northern Chile [4], we identified enriched trace elements. Moreover, we used x-ray diffractometry and scanning electron microscopy to assess the mineralogical and elemental compositions of the impurities. The single particles were assigned to reflectance spectra using hyperspectral imaging microscopy. For each ice sample, the spectral reflectance was measured *in situ*. We produced an albedo map from a Landsat satellite image from roughly the same day than the field survey (Fig. 1) for a glacier and catchment assessment.

The results showed high concentration of mineral dust (99 % of the total mass). Dust flux per square meter was roughly 10 times higher at OB in comparison to Patagonia or the Canadian Arctic, but comparable to the Tien Shan [5]. All samples had similar mineralogical composition. The main minerals are the ones found in metamorphic rocks with granitic composition, e.g. gneisses with quartz, albite, muscovite and chlorite. Traces of heavy metals such as oxidized iron and titanium were distributed throughout the analyzed samples (OA and PN). The dominant minerals (e.g. quartz and muscovite) show a relatively high reflectance. Oxidized iron and titanium lowered the spectral reflectance of the single particles. The heavily enriched trace elements

Cu, Co, Mo and Pb at OA and PN are attributed to anthropogenic pollution. Field based albedo values are higher than satellite derived albedos (Fig. 1).

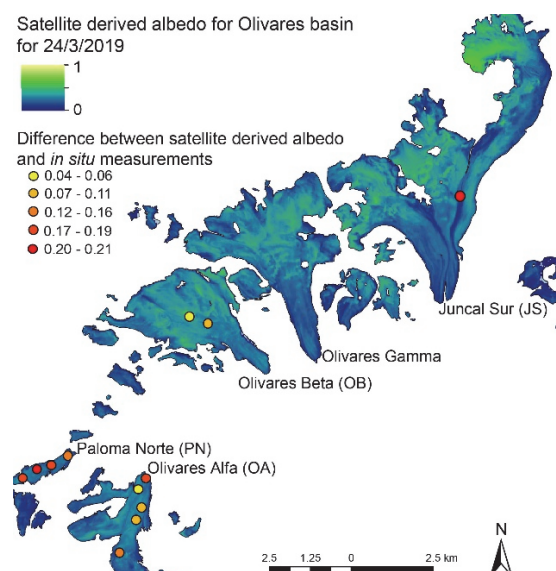


Fig. 1: Surface albedo map from Landsat compared to *in situ* albedo measurements for the Olivares basin.

The enrichment of certain trace elements (Cu, Co, Mo), iron and titanium coating and heterogenous element distribution supports a potential anthropogenic contribution on deposited impurities from mining activity. Elevated EC concentrations were found in the OA samples, as well as enrichment of Ni originating most likely from pollution of Chile's capital city Santiago. OA (-0.85 ± 0.1 m w.e. yr⁻¹) and PN (-0.97 ± 0.1 m w.e. yr⁻¹), two glaciers in the immediate surrounding of the mines, lost substantially more mass than JS (-0.27 ± 0.05 m w.e. yr⁻¹) that agrees better with the regional mass loss [6]. However, the quantification of anthropogenic induced effects on glacier-wide albedo through LAI input and hence on glacier melt remains unresolved.

We acknowledge funding from the Centro de Estudios Científicos, Valdivia, Chile.

- [1] M. Zemp et al., *Nature*, **568**, 382–386 (2019).
- [2] M. Huss and R. Hock, *Nat. Clim. Change*, **8**, 135–140 (2018).
- [3] P. M. Rowe et al., *Sci. Rep.*, **9**, 1–16 (2019).
- [4] V. Oliveros et al., *Andean Geology*, **34**, 209–232 (2007).
- [5] N. Takeuchi and Z. Li, *Arct. Antarct. Alp. Res.*, **40**, 744–750 (2008).
- [6] I. Dussaillant et al., *Nat. Geosci.*, **12**, 802–808, (2019).

CARBONACEOUS AEROSOL TRENDS AND SOURCES FROM AN ALPINE ICE CORE

L. Fang (PSI & Univ. Bern), F. Cao (NUIST), S. Henne (EMPA), S. Szidat (Univ. Bern),
M. Schwikowski (PSI & Univ. Bern), T. M. Jenk (PSI)

Alpine ice cores allow access to continuous records of atmospheric composition back to the pre-industrial era in the regions where the majority of humans live. Here we present 340-year concentration records of organic carbon (OC), and elemental carbon (EC) separated into fossil and non-fossil contribution using the ^{14}C content.

The impact of aerosol particles on the Earth's radiation balance remains poorly constrained, leading to considerable uncertainties in predicting the climate sensitivity to greenhouse gases. A large part of these uncertainties is related to the deficient knowledge of the magnitude of pre-industrial emissions [1], particularly for carbonaceous compounds forming a major fraction of the atmospheric aerosol. One of the most important approaches to constrain the pre-industrial aerosol burden is to obtain records from ice cores. The Fiescherhorn ice core (Swiss Alps) was drilled in 2002, is 150.5 m long and well dated back to 1660 by annual layer counting [2]. Total carbonaceous aerosol concentration (sum of OC and EC) increased by a factor of three at the end of 20th century compared to the pre-industrial background. Radiocarbon based source apportionment shows that fossil fuel combustion contributed up to ~35 % of enrichment.

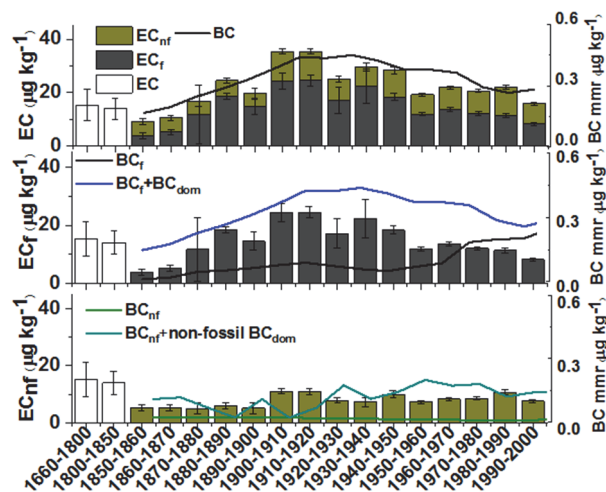


Fig. 1: Comparison between the EC concentration in ice core and atmospheric BC load in 10-year resolution.

EC has highest values in the first half of the 20th century (Fig. 1), to a large extent caused by fossil fuel emissions. The estimated BC atmospheric mass mixing ratio (mmr) from FLEXPART model based on emission inventory is comparable with the ice core record. Domestic BC emissions share the same trend with fossil EC, which suggests that domestic emissions were dominated by fossil sources for the period of 1880-1950. The excess of the sum BC_f and BC_{dom} compared to EC_f is

attributed to non-fossil BC_{dom} , which is the main source of EC_{nf} .

OC shows a strong increasing trend between 1940 and 1980, mostly of non-fossil origin. The fossil OC (OC_f) trend is well explained by primary OC emissions and fossil NMVOC emissions. In contrast, the increase in non-fossil OC is not visible in the emission estimates of OC with a mismatch of up to one magnitude a factor of five in the second half of the 20th century.

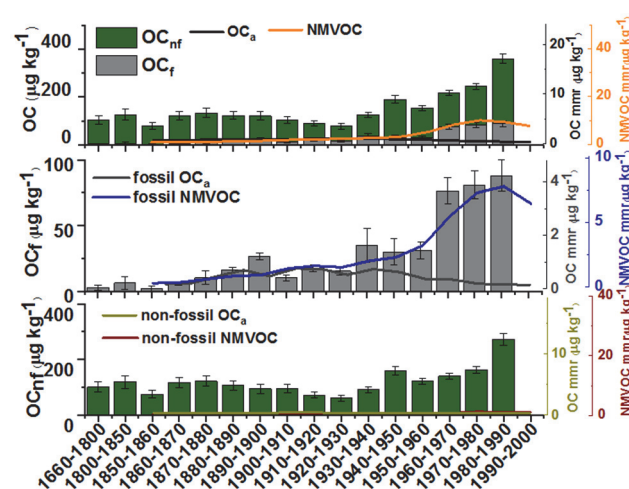


Fig. 2: OC concentrations from fossil and non-fossil sources over the period of 1680-1990.

The comparison between the ice core records with emission inventories indicates that emission data of BC agree well with EC observations, but OC emissions underestimate the OC aerosol. We attribute this trend primarily to enhancement of SOA formation caused by the presence of anthropogenic precursor gases or by the increase of the atmospheric oxidative capacity. Thus, bottom-up emission inventories seem to underestimate heavily the atmospheric OC loading by not accounting adequately for SOA formation, limiting the capacity of current models in estimating anthropogenic aerosol forcing.

We acknowledge the Laboratory for the Analysis of Radiocarbon with AMS (LARA) for support with radiocarbon measurements.

- [1] K. Carslaw et al., *Nature*, **503**, 67-71 (2013).
- [2] T. M. Jenk et al., *Atmos. Chem. Phys.*, **6**, 5381-5390 (2006).

A NEW DATING TOOL FOR ALPINE ICE BASED ON DO¹⁴C

L. Fang, T. Singer (PSI & Univ. Bern), S. Hou (Univ. Nanjing), T. M. Jenk (PSI), M. Schwikowski (PSI & Univ. Bern)

Recent improvements in radiocarbon analysis techniques allowed us to develop a new ice dating method based on ¹⁴C in dissolved organic carbon (DOC) in glacier ice. Ice samples from four different locations were analysed to evaluate the DO¹⁴C dating method.

A precise age-depth relationship in ice cores is essential for paleoclimate studies. Radiocarbon dating of water insoluble organic carbon (WIOC) has become an important dating tool to constrain the age of ice cores from nonpolar glaciers, and the accuracy of this method has been validated recently [1]. However, in some cases this method is restricted by the low WIOC concentrations (10-60 ppb) present in the ice [2]. Considering the comparably higher concentrations of DOC (50-100 ppb) [3], radiocarbon dating using DOC will generally demand less ice sample mass and may allow dating even when the WIOC concentration is too low.

To validate the dating using DO¹⁴C, the deep part of ice cores from four different glaciers - Colle Gnifetti, Belukha, Chongce, and Shu Le Nan Shan (SLNS) - were selected (Fig. 1). Each sample was ¹⁴C dated using both the DOC and WIOC fraction to allow a direct comparison of the two methods. Samples are melted and further cleaned by rinsing with ultra pure water in a melting vessel, all under helium inert gas conditions. WIOC is then separated by filtration and inorganic carbon (IC) is removed from the filtrate via acidification and degassing with helium. The remaining DOC in the solution is oxidized by two UV lamps in a quartz glass photo-reactor. Produced CO₂ is collected by cryogenic traps, purified, quantified and finally flame-sealed in glass vials for ¹⁴C analyses [4].

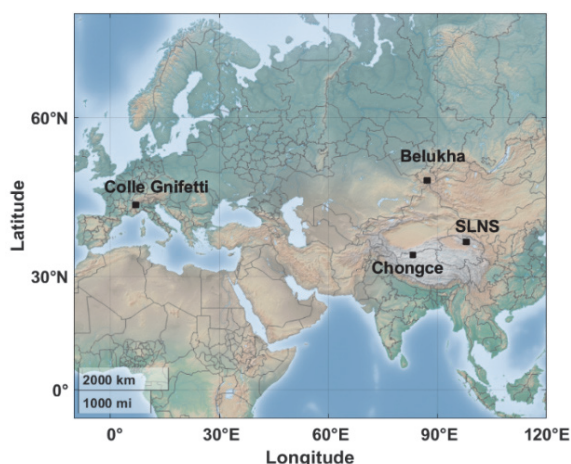


Fig. 1: Location of the four glaciers sampled.

On average, DOC concentrations ($187 \pm 180 \mu\text{g carbon per kg ice}$) were about two times higher than WIOC concentrations ($106 \pm 44 \mu\text{gC kg}^{-1}$). This is consistent

with previously reported ratios [3]. Comparing the obtained DO¹⁴C ages with WIOC ¹⁴C ages, we found all samples to scatter around the 1:1 ratio line (Fig. 2). The linear regression shows good agreement between the two dating methods, although WIOC ages seem to indicate a significant systematic shift to older ages for sample younger than ~1000 year. This possibly indicates an incomplete removal of carbonates (¹⁴C dead) from the WIOC fraction. Based on ¹⁴C mass balance, a contribution of ~1.7 μgC from remaining carbonates was calculated causing the observed offset. This would conclude that although more than 95 % of all carbonates is usually removed from the filter by the applied acidification step the remaining 5 % are critical.

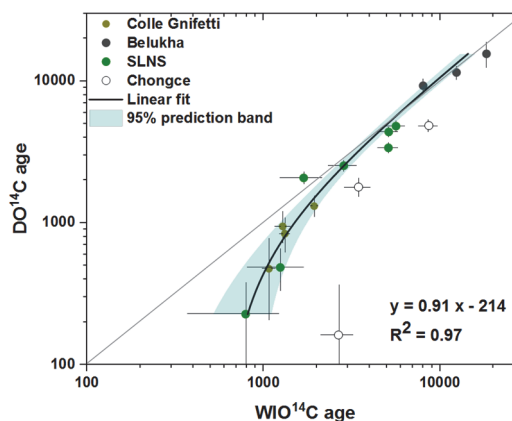


Fig. 2: Comparison of DOC and WIOC ¹⁴C ages. Shown ¹⁴C ages are given as the mean age: $\mu \pm 1\sigma$ range.

In summary, our results indicate that DOC and WIOC yield comparable ¹⁴C ages. However, a systematic bias to older ages in the WIOC fraction seems apparent, likely related to carbonates from mineral dust. At least for sites experiencing exceptionally high loading with mineral dust (e.g. Chongce, see Fig. 2), an improved carbonate removal procedure thus seems to be required. In any case, this study clearly demonstrates the benefit of using the DOC fraction as an additional, independent tool for the dating of high-alpine ice cores.

We acknowledge the Laboratory for the Analysis of Radiocarbon with AMS (LARA).

- [1] C. Uglietti et al., *The Cryosphere*, **10**, 3091-3105 (2016).
- [2] T. M. Jenk et al., *J. Geophys. Res.*, **114**, D14305 (2009).
- [3] M. Legrand et al., *J. Geophys. Res.*, **118**, 3879-3890 (2013).
- [4] Fang et al., *Radiocarbon*, **61**, 681-694 (2019).

MATCHING OF THREE DIFFERENT COLLE GNIFETTI ICE CORES

T. Singer, A. Rieder (PSI & Univ. Bern), S. Brüttsch, T. M. Jenk (PSI), P. Nalivaika, L. Fang (PSI & Univ. Bern), A. Eichler (PSI), M. Schwikowski (PSI & Univ. Bern)

A cross-comparison based on the records of NH_4^+ and $\delta^{18}\text{O}$ of different ice cores from the well-studied site Colle Gnifetti in the Monte Rosa massif (Swiss Alps) is presented.

Ice sheets and glaciers are valuable natural archives that contain information about the history of the Earth's atmosphere. Ice cores from high-altitudes glaciers at lower latitudes are of growing interest because of their geographical proximity to human activities, providing information to study related atmospheric pollution and processes (e.g. aerosol from the combustion of fossil fuels). The Colle Gnifetti (CG, 4455 m asl.), a glacial saddle between Zumsteinspitze and Punta Gnifetti, is located in the uppermost part of the accumulation area of Grenzletscher, surrounded by the highly industrialised area of Central Europe. As this glacier saddle is located at a high altitude, the stability of the atmospheric layering during the winter season limits the transport of air from the emission sources to the study site, resulting in seasonal variations. For some compounds, this variation is further enhanced by the seasonality of the emission source strength (e.g. $\text{NH}_3/\text{NH}_4^+$ from biological activity and agricultural fertilization). The isotopic fractionation of the stable isotopes of water ($^{16}\text{O}/^{18}\text{O}$, $^1\text{H}/^2\text{H}$) is a temperature-dependent process and underlines the seasonal variations by reflecting winter as minima and summer as maxima. The presence of these seasonal cycles is the basis for the ice core dating by incremental annual layer counting (ALC).

We compared the records of major ions and stable isotopes of water (expressed as $\delta^{18}\text{O}$ and δD) from the ice cores drilled in 2015 (CG15) and 2003 (CG03, [1]), aiming to achieve synchronisation and a common, overlapping age scale. A firm core from the same site, obtained in 2008 (CG08) was used for additional constraint. The distance between the three sites is ~ 20 m. Concentrations of major ions were determined by ion chromatography (850 Professional IC, Metrohm) and the stable isotopes of water by Wavelength-Scanned Cavity Ring-Down Spectroscopy (WS-CRDS, Picarro). The ALC of the CG15 was performed using the Core-Dating [2] software tool, mainly considering the signals of NH_4^+ and $\delta^{18}\text{O}$. The CG15 and CG08 records of major ions and $\delta^{18}\text{O}$ were then aligned to the established chronology of CG03. The alignment of the cores was performed using the CoreMatch [3] software tool. The temporal variability of mineral dust, with calcium used as a proxy, and particularly the pronounced layers from events of long-range transport of Saharan dust (SDE), served as absolute tie points for core matching (Fig 1).

Fig. 2 shows a comparison of the $\delta^{18}\text{O}$ records from the three cores after alignment. The signals are in good agreement, but deviations in the fine structure, most often observed in a missing of pronounced minima related

to winter snow, are evident. This characteristic underlines the difficulty of dating alpine ice cores, particularly at a site like CG with preferential wind erosion of cold, light winter snow. Although annual accumulation rates at CG seem to vary quite substantially even within a few meter, these results show that ice cores from the same location similarly record information at least on a multi-annual scale. However, it also underlines, that particularly for a site like CG a stacked record from multiple cores may result in a more complete picture of past pollution and climate.

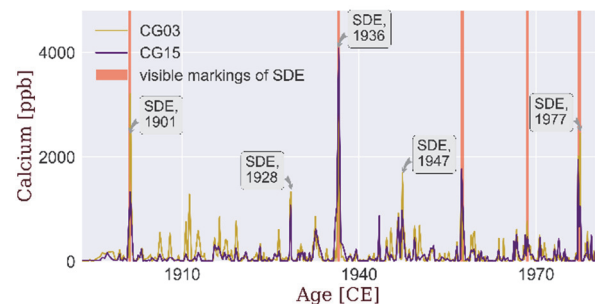


Fig. 1: Comparison of the calcium records of the CG15 (purple) and CG03 (green) ice cores. Visible dust layers are marked by yellow bars. SDE used as tie points are denoted.

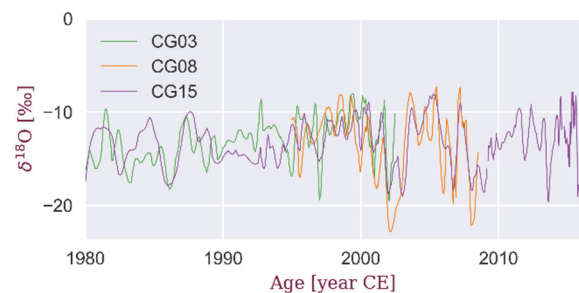


Fig. 2: Comparison of the $\delta^{18}\text{O}$ records of CG15, CG08, and CG03 over the last decades. The CG15 and CG08 records are aligned to the chronology of CG03 for the overlapping period.

We acknowledge funding from the Swiss National Science Foundation (Grant 200021_182765).

- [1] T. M. Jenk et al., *J. Geophys. Res.-Atmos.*, **114**, D14305 (2009).
- [2] A. V. Kurbatov, *American Geophysical Union*, **86** (2005).
- [3] Adapted from K. McGwire, Desert Research Institute, Reno.

THE ADAMELLO ICE CORE – DATING WITH A TWIST

T. M. Jenk (PSI), M. Schwikowski (PSI & Univ. Bern), V. Maggi (Univ. Milano), D. Festi (unibz)

Within the framework of the CALICE – Calibrating Plant Biodiversity in Glacier Ice – project, a 45 m ice core was extracted from the Adamello glacier (Italian Alps). Here we report on the successful dating of this core, marking a crucial project achievement.

The Adamello glacier is a temperate glacier, characterized by ice temperatures at the pressure melting point, and therefore affected by melting and percolation processes. The 2016 coring site at Pian di Neve (3200 m asl.), a plateau in the accumulation zone of the glacier, was selected in the area of maximal glacier ice thickness. With 240 m of ice, this site potentially allows access to paleo-records of several hundred years. However, such records are only valuable in case the proxy signals of interest remain unaffected by post-depositional processes and can be placed in a chronological context. Because of meltwater percolation occurring in temperate glacier ice, proxies such as soluble ions will be disturbed by wash-out effects. Particularly for the time of recent warming, such glaciers may further experience years with negative mass balance even in the accumulation zone. This may cause a surface loss of annual layers, leaving the glacier ice surface to be of unknown age at the time of sampling. So far, only a few ice cores from temperate glaciers could successfully be dated, with the environmental radionuclide ^{210}Pb showing to be a crucial dating tool [1].

The Adamello ^{210}Pb ice core profile did not show the typical decrease in activity concentrations with depth, expected due to the radioactive decay of ^{210}Pb incorporated with snow fall ($T_{1/2} = 22.3$ a). Instead, a value of 692 mBq kg^{-1} was observed in the upmost sample, high compared to usually $\sim 100\text{ mBq kg}^{-1}$ in freshly deposited annual surface snow in the European Alps [1]. Samples below showed a pattern, resembling the profile of a closeby ice core drilled on Silvretta glacier in 2011 (SI, 2930 m asl., Eastern Swiss Alps); one of the few dated ice cores from a temperate glacier [2] (Fig. 1).

Besides ^{210}Pb , the Adamello ice core has so far been analysed for pollen, black carbon (BC) and ^{137}Cs . ^{137}Cs is tightly bound to insoluble particulate matter and thus assumed to be rather unaffected by percolating meltwater (no significant relocation or removal). Its profile in the Adamello ice core revealed two distinct peaks [3]. One at 27.1 m w.e. depth, related to the nuclear fallout from atmospheric nuclear tests with a maximum in 1963, the other at a shallower depth of 6.6 m w.e., a potential signal from the 1986 Chernobyl accident. In the SI ice core, the 1963 horizon was detected by the ^3H peak found at 28.9 m w.e. depth. As shown in figure 1, we shifted the depth of the SI ice core to align the 1963 horizons found in both cores.

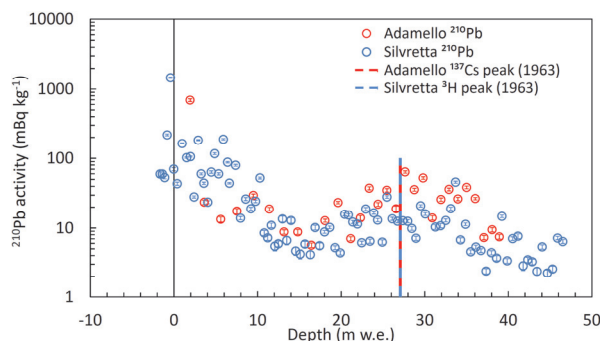


Fig. 1: ^{210}Pb profiles of the Adamello and Silvretta ice cores, aligned by the 1963 horizon.

With the ^{210}Pb profiles showing reasonable alignment by doing so, the SI age scale could directly be applied to the Adamello ice core (Fig. 2). Unexpectedly, the resulting chronology precisely matched the ^{137}Cs peak attributed to 1986. For the surface age of the Adamello glacier at drill date, this approach leads to the year 1998 ± 3 . This agrees well with 2001 ± 4 , the year estimated based on the high ^{210}Pb surface sample value assumed to reflect enrichment at the surface when ice melted, and thus representing an integrated activity (Fig. 2). Last, ALC based on distinct minima and maxima in pollen and BC, allowed for an independent dating, confirmed the chronology for 1963-1986 by a tight match and indicated reasonable signal preservation of these proxies (Fig. 2). ALC resulted in a slightly lower surface age, relating it to summer 1993. Overall, this accounts to recent surface loss equal to around 20 years of deposition.

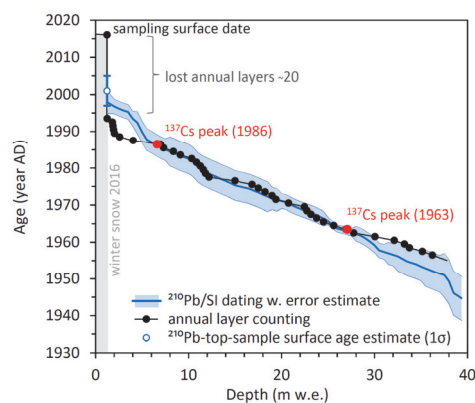


Fig. 2: Independent dating results and surface age estimates for the Adamello ice core.

We acknowledge funding from the EVTZ/Austrian Science Fund (Grant IPN57-B22).

- [1] H. W. Gäggeler et al., *J. Glaciol.*, 1-10 doi.org/10.1017/jog.2020.19 (2020).
- [2] P. Pavlova et al., *ES&T*, **49**, 14085–14091 (2015).
- [3] E. Di Stefano et al., *J. Environm. Radioact.*, 208-209, D106039 (2019).

THE AGE OF ICE OF RHONE GLACIER – ICE FLOW MODELING AND ^{14}C DATES

*J. Morgenthaler (ETHZ), T. M. Jenk (PSI), G. Jouvét (ETHZ & Univ. Zürich),
M. Schwikowski (PSI & Univ. Bern), A. Bauder (ETHZ)*

Glacier ice flow models can potentially be constrained by spot-wise availability of absolutely dated ice in the glacier body. Here we present first results from Rhone Glacier (2300-3450 m asl., Swiss Alps).

The movement of a temperate alpine glacier occurs from plastic ice deformation (shearing) and basal ice sliding [1]. These two processes cannot be distinguished at the surface, e.g. by direct glacier surface velocity observations. In this study, the effect of basal motion on surface ice isochrones was investigated by a numerical modeling approach. Further, the age of ice in a core extracted at the terminus of Rhone Glacier in 2017 was estimated, using modelled back-trajectories of ice particles. For comparison, samples from this core were ^{14}C dated. The setting of the study site is shown in Fig. 1.

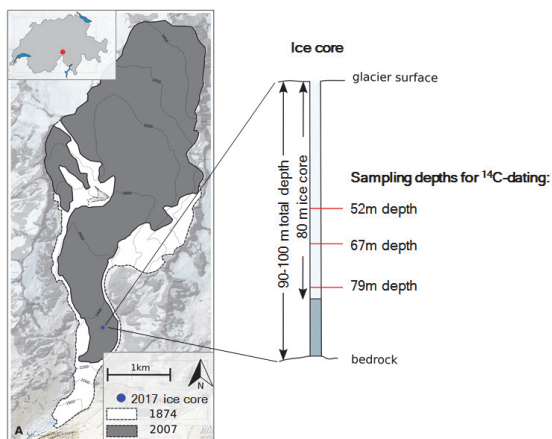


Fig. 1: Rhone Glacier drill site (blue dot) and ice core ^{14}C sampling depths. White and gray areas indicate the glacier extent in 1874 and 2007 respectively.

The parallel and finite element code Elmer/Ice was used for modelling the dynamics and evolution of Rhone Glacier [2]. Ice deformation was described by Glen's flow law while basal friction was treated using Weertman's bedrock sliding law. A diagnostic model (in 2D and 3D) with steady ice geometry served to investigate conceptually how the shearing to sliding ratio influences the surface age distribution. In a prognostic model setup (3D), to model trajectories of ice particles backward in time, Elmer/Ice was coupled to a mass balance model and the temporal evolution of changing ice geometry considered. Ice core samples from three depths were ^{14}C dated, using the particulate organic carbon fraction contained as impurities in the ice [3] (Fig. 1).

The diagnostic modeling indicates that 20-30 years older surface ages are to be expected in the ablation zone with basal sliding allowed compared to the non-sliding case. With the prognostic model, using boundaries for changing glacier extent as observed between 1874 and 2007, the modeled back trajectories yield an emergence of the ice core particle in the accumulation

zone of Rhone Glacier. For particles from the top and bottom of the ice core, the mapped trajectories are nearly similar, except ~ 50 years prior to emergence. Ice particles were deepest ~ 100 years after deposition at up to 400 m below glacier surface. The time between ice/snow particle deposition and arrival at the ice core location (i.e. the modeled age of ice in the core) results with 212 and 194 years for the bottom and top part of the ice core, respectively (Fig. 2). ^{14}C dating of ice samples gave ages of 350-870, 320-870 and 340-1000 years for the depths of 52 m, 67 m and 79 m, respectively (1σ -range). While modeling and absolute dating agree that the age difference between ice core top and bottom ice is relatively small (i.e. insignificant for ^{14}C), the dating by ^{14}C generally suggest at least slightly older ages. However, the achieved precision does not allow evaluating or even constraining the model output. Reducing the ^{14}C -dating uncertainty and trying to assess model uncertainty and sensitivity to changes in free model parameters could be the subject of a future project.

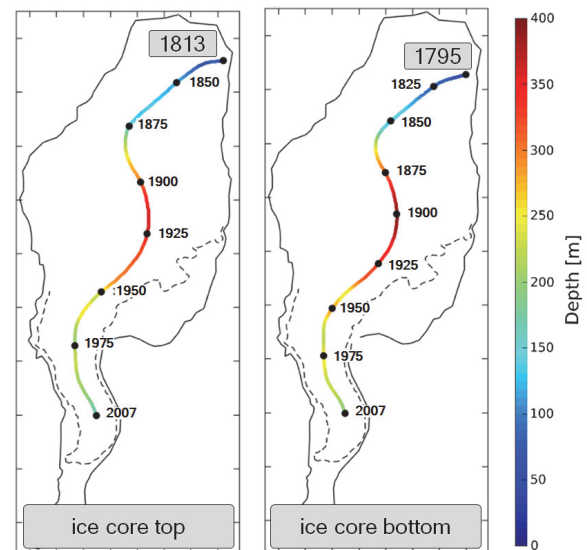


Fig. 2: Modeled backward trajectories starting from ice core top and bottom depth. Location and time of emergence indicate modeled deposition origin and deposition time, respectively. Colors indicate depth below glacier surface.

We acknowledge funding from the Swiss National Science Foundation (Grant 200021_169329).

- [1] K. Cuffey and W. Patterson, *The physics of glacier*, 4th edition, Elsevier (2010).
- [2] O. Gagliardini et al., *Geoscientific Model Development*, **6**, 1299–1318 (2013).
- [3] T. M. Jenk et al., *JGR*, **114**, D14305 (2009).

TOWARDS CROSS-DATING OF TWO ICE CORES FROM THE MONGOLIAN ALTAI

*P. Nalivaika, L. Marti, T. Singer (PSI & Univ. Bern), S. Brütsch, T. M. Jenk (PSI),
M. Schwikowski (PSI & Univ. Bern), A. Eichler (PSI)*

For assessing recent heavy metal pollution from the territory of the former Soviet Union (FSU), dating of a 52 m long ice core from the Mongolian Altai is crucial. Our results show exceptionally good agreement in chemical records between the studied ice core and a well-dated 72 m parallel core, allowing future cross-dating of the two cores.

Atmospheric pollution by heavy metals and, in particular, by Pb presents a significant issue because of its hazardous effect on human health. Whereas recent Pb pollution is well documented for many regions worldwide, existing Pb records for the territory of the former Soviet Union (FSU) demonstrate some controversy. Officially reported Pb emission estimates for the period 1990–2007 show a decreasing trend [1], while Pb concentrations obtained from a Tien Shan ice core (influenced by emissions from the FSU and China) increased during the 1990s [2]. We will reconstruct recent FSU Pb and other heavy metal emissions based on an ice core from the Mongolian Altai (Tsambagarav mountains). In 2009, two parallel ice cores (52 m and 72 m length, distance few m) were drilled at the Tsambagarav site. The 72 m core was dated earlier, covering the period 2009 AD – 4800 BC [3]. However, no material was left for acquiring records of heavy metal pollution. For this purpose the 52 m parallel core will be used. Since this core is not dated so far, the aim of this study is to perform a cross-dating of the 52 m and 72 m parallel cores based on a comparison of major ion records.

So far, the upper 43 m (32 m w.eq.) of the 52 m Tsambagarav ice core were sampled with a resolution of 5 cm and analyzed for major ions and water stable isotopes. Concentrations of major ions were analysed with ion chromatography (Metrohm 850 Professional). Determination of water stable isotope ratios was performed using Wavelength-Scanned Cavity Ring-Down Spectroscopy (WS-CRDS, Picarro L2130-i). Obtained records were compared with those from the well-dated 72 m Tsambagarav ice core. Records of the two parallel cores agree exceptionally well for water stable isotopes ($\delta^{18}\text{O}$, δD) and anthropogenically derived species (such as NH_4^+ , NO_3^- , and SO_4^{2-}) (see Fig. 1). For dust-related ions (such as Ca^{2+} and Mg^{2+}), larger differences occur due to inhomogeneity in dust deposition, but distinct maxima (e.g. at 11.6 m w.eq.) are the same in both cores. Unlike at many other study sites, variations in water stable isotope signals ($\delta^{18}\text{O}$) shown in Figure 1 cannot be solely explained by changing temperatures, but are most probably also affected by fluctuations in precipitation [4]. NH_4^+ is an important proxy for biogenic and anthropogenic emissions that can be used to distinguish different seasons. Thus, unsmoothed NH_4^+ and $\delta^{18}\text{O}$ records allow dating of the ice core based on annual layer counting (ALC) using seasonal variations

of the signals. The upper 43 m (32 m w.eq.) cover the period 1861–2009 AD.

In order to complete the cross-dating of the two ice cores, chemical records will be further adjusted and matched using specialized software (CoreMatch and ALC – Ice Core Dating Tool). The dated 52 m core will then be used to reconstruct recent FSU metal pollution.

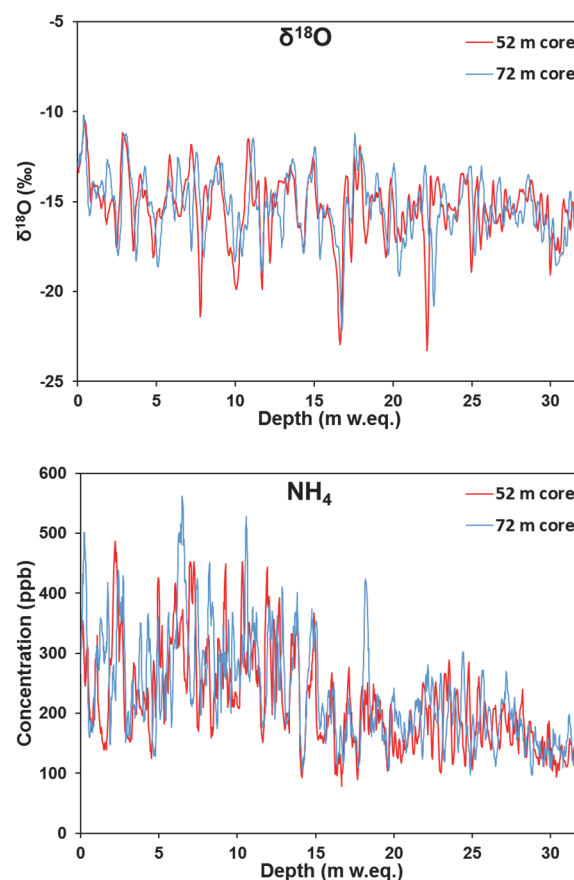


Fig. 1: $\delta^{18}\text{O}$ (top) and NH_4^+ records (bottom) for the parallel 52 m and 72 m Tsambagarav ice cores. Shown are 5- and 10-point moving averages, respectively, to account for the different sampling resolution of 5 and 2.5 cm, respectively.

We acknowledge funding from the Swiss National Science Foundation (Grant 181985).

- [1] HELCOM, <http://www.helcom.fi/>.
- [2] B. Grigholm, et al., *Atmos. Environ.*, **131**, 17 (2016).
- [3] P. A. Herren et al., *Quaternary Sci. Rev.*, **69**, 59 (2013).
- [4] P. A. Herren, PhD Thesis, University of Bern (2013).

CHERNOBYL HORIZON IN A CENTRAL ASIAN ICE CORE

A. Eichler (PSI), M. Kronenberg (Univ. Fribourg), S. Brüttsch (PSI), M. Rütli, M. Heule (PSI ASI),
M. Schwikowski (PSI & Univ. Bern), H. Machguth, M. Hoelzle (Univ. Fribourg)

A maximum in total β -activity associated with the fallout from the Chernobyl nuclear reactor accident in 1986 helped to refine ice core dating of an 18 m core from Gregoriev ice cap in Kyrgyzstan.

The reconstruction of past climate and pollution from ice core records crucially depends on a precise dating of the core. For establishing age-depth scales of ice cores covering the last decades annual layer counting based on seasonally varying concentrations of impurities such as NH_4^+ is the method of choice [1]. However, often the assignment of annual layers is not unambiguous and further dating horizons are needed.

Here we report on measurements of the ^{137}Cs γ - and total β -activity in an 18 m ice core from Gregoriev ice cap in Kyrgyzstan, drilled in 2018. The initial motivation for the drilling was the investigation of firm and mass balances changes in this data sparse region. Dating of the core by annual layer counting using NH_4^+ and density records yielded an age of the bottom layers of ~ 40 years (± 10 years). The huge dating uncertainty is partly due to meltwater influence, to some extent disturbing chemical records. Thus, the aim of this work was to find a reference horizon to refine the dating. Therefore, we looked for a maximum in ^{137}Cs γ -activity and/or total β -activity that can be related to the fallout from the Chernobyl nuclear power station accident in April 1986.

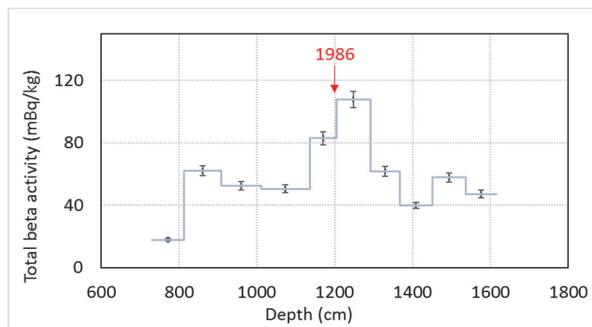


Fig. 1: Total β -activity in ten filtered samples from Gregoriev ice core, shown is the difference to the blank value and the 2σ uncertainty.

For the activity measurements, ten ice core samples in the depth range between 7 and 16 m and 1 blank sample (frozen MilliQ water) were prepared. Each sample consisted of 1 kg of ice, acidified in a 1 L plastic container with 0.33 ml of concentrated HCl [2]. Samples were melted at room temperature. In a first attempt, we measured the ^{137}Cs γ -activity directly in the container, using a GMK γ -detector. However, even after 24 h of analysis, measured γ -activities remained below the detection limit (DL) of ~ 1400 cph/kg (0.4 Bq/kg). In a second attempt, we pre-concentrated radionuclides from the acidified samples using MN616 LSA-50 cation exchange

filters. Every sample was filtered three times and subsequently, the filters were dried at 60°C . ^{137}Cs γ -activity on the filters was determined during a 24 h measurement using a GMK γ -detector. Despite the improved DL of 110 cph/kg (0.03 Bq/kg), measured ^{137}Cs γ -activities did not significantly exceed the DL. Additionally, the filters were analyzed for total β -activity. Each sample was measured six times 1 h at a LB790 detector. Blank corrected total β -activity background signals fluctuate between 18 and 60 mBq/kg (Fig. 1). Two samples show enhanced activities of 83 and 108 mBq/kg. The observed maximum between 11.4 and 13 m is also evident in the dust-normalized β -activities (not shown). Retention of radionuclides strongly depends on the total quantity of insoluble matter. Since we did not measure insoluble particle content, Ca^{2+} was used for normalization, assuming that insoluble particle signals and Ca^{2+} concentrations are often highly correlated [3].

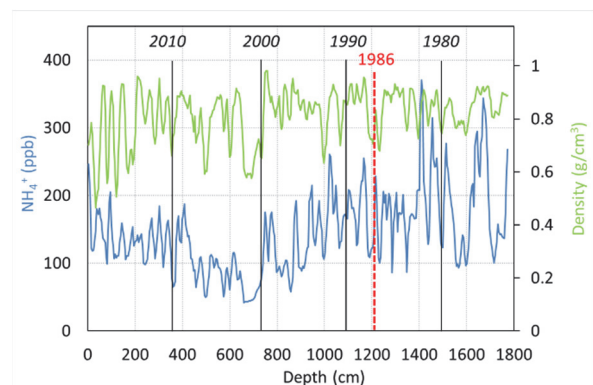


Fig. 2: Records of NH_4^+ concentrations (blue) and densities (green) (3 point moving averages) in the 18 m Gregoriev ice core. The detected Chernobyl horizon is marked in red and dating based on annual layer counting is indicated with black lines and italic numbers.

Based on the maximum β -activities in two samples, we conclude that fallout from the Chernobyl accident is included in both samples. Thus, we can assign the depth of 12 m to the year 1986 (Fig. 1). With this reference horizon, we were able to refine the dating of the ice core (Fig. 2). Accordingly, the 18 m core covers the period from 1974(± 3) to 2018. With the precise dating, ice core variations in annual accumulation rates will now be investigated to study glacier mass balance changes at the Gregoriev ice cap.

We acknowledge funding from the Swiss National Science Foundation (Grant 200021_169453).

- [1] A. Eichler et al., *J. Glac.*, **46**, 507 (2000).
- [2] H. ShuGui et al., *Chin. Sci. Bul.*, **52**, 428 (2007).
- [3] P. Bohleber et al., *Clim. Past*, **14**, 21 (2018).

DETERMINING THE AGE OF THE ICE IN THE MURTÈL ROCK GLACIER

V. Bella (PSI), A. Cicoira, I. Gärtner-Roer, A. Vieli (UZH), T. M. Jenk (PSI), M. Schwikowski (PSI & Univ. Bern)

Rock glaciers are defined as bodies of frozen debris with interstitial ice cement, ice lenses and/or a core of massive ice [1]. They are a common feature in the European Alps [2]. Whether they are formed by permafrost creep, talus deformation (rockslide) or simply are permafrost and debris protected relicts of glaciers is still under debate (e.g. [3]). The aim of this project is to determine the age of the Murtèl rock glacier and potentially to improve the understanding of rock glacier formation.

The Murtèl rock glacier is located near the Piz Corvatsch in the Upper Engadin (2670 m asl., Eastern Swiss Alps) [1]. Previous research has been conducted on a core drilled in 1987. Radiocarbon dating of macrofossils (moss) showed an age of 2250 ± 100 at 5.94 m depth [2]. For renewal of the PERMOS [4] borehole, a new core was retrieved in 2015 from the ice rich part (49 core segments). Planned analysis include visual stratigraphy, ^{14}C dating of water-insoluble organic carbon (^{14}C -WIOC) by accelerator mass spectrometry as well as measurements of stable isotopes of water ($\delta^{18}\text{O}$ and δD , cavity ring-down spectroscopy) and concentrations of major ions (ion chromatography). So far, data are available for sections 11 and 30 (Table 1). Section 44 from a depth of 29.60 m is a piece of solid rock with a density of $\sim 2.4 \text{ g cm}^{-3}$, identified to be of granitic composition. Whether this is a piece of an ice-incorporated boulder or bedrock is unknown. Core segments below this depth will help to draw firmer conclusions.

Table 1: First ^{14}C dating results for sections 11 and 30.

No.	Mid-depth	Stratigraphy	Age
11	11.40 m	Relatively compact and clean milky ice with a 5 cm sand layer of brownish colour.	2999 ± 646 cal yr BP
30	21.80 m	Very coarse-grained ice, particles/debris (2-3 cm \emptyset).	4736 ± 753 cal yr BP

In Fig. 1, the derived ages from Murtèl are compared to those from the active rock glacier Lazaun in the southern Ötztal Alps [5]. The ages are slightly younger for Murtèl, but show comparable increase with depth. A preliminary calculation of the annual layer thickness in the Murtèl rock glacier yields $\sim 6 \text{ mm yr}^{-1}$.

For water stable isotope analysis, samples were cut in 5 cm resolution, corresponding to ~ 8 years if considering the derived annual layer thickness. The $\delta^{18}\text{O}$ average value is -14.0 ‰ and -15.0 ‰ for section 11 and 30, respectively. Despite the lower elevation, these values are slightly lower than the 11-year mean of -12.2 ‰ observed in the nearby ice core from Piz Zupó (3870 m asl.) [6]. This might indicate a different accumulation/deposition process, a predominant recording of the

winter signal in the rock glacier or relate to lower temperatures at the time of deposition. At Piz Zupó, the seasonal variation is around 10 ‰ whereas the variability in the Murtèl samples is only 1.5 ‰ , which is comparable considering the smoothing resulting from the applied multi-annual sampling resolution.

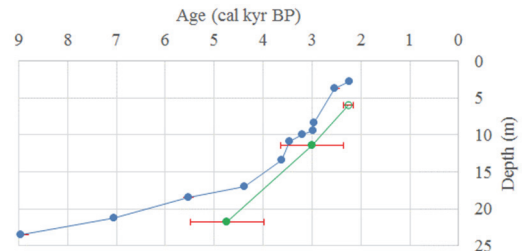


Fig. 1: Age-depth relationship for the Lazaun (blue) and Murtèl (green, open symbol: [2]) rock glacier with the 1σ range (red).

Major ions have so far been analysed for core section 11 (clean, in-transparent ice; Fig. 2). For this section, concentrations in the Murtèl samples are generally lower compared to the average concentrations in the Piz Zupó ice core. This is true even for dust related tracers such as calcium.

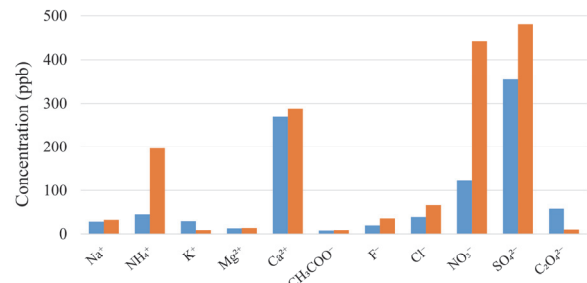


Fig. 2: Concentrations of major ions for Murtèl (section 11, blue) compared with 11-yr average values for Piz Zupó (orange).

This study will continue with the analysis of water stable isotopes and ^{14}C -WIOC on the remaining and major ions on a selected few ice sections, respectively.

- [1] W. Haerberli et al., Arbeitsheft Nr. 9, ETH Workshop Report (1990).
- [2] W. Haerberli et al., *J. Glaciol.*, **45**, 1-8 (1999).
- [3] W. B. Whalley and H.E. Martin, *Prog Phys Geogr*, **16**, 127-186 (1992).
- [4] The Swiss Permafrost Monitoring Network
- [5] K. Krainer et al., *Quaternary Res.*, **83**, 324-335 (2014).
- [6] A. Palmer et al., *Annual Report LCH-PSI*, **30** (2005).

THE INFLUENCE OF ACIDIFICATION TIME ON TRACE ELEMENT ANALYSIS

T. S. Münster (PSI & Univ. Bern), T. M. Jenk (PSI), C. J. Huber (PSI & Univ. Bern), A. Eichler (PSI), P. Nalivaika, M. Schwikowski (PSI & Univ. Bern)

Trace element (TE) concentrations in an ice core, analysed with different systems (ICP-SF-MS and ICP-TOF-MS) showed similar trends, but a difference in the absolute values for some TEs [1]. One reason for this could be the difference in the applied time of sample acidification prior to analysis, which we tested here.

TEs in the atmosphere originate from natural and anthropogenic sources. The analysis of TEs is usually performed by inductively coupled plasma mass spectrometry. Samples of ice cores are first melted, acidified and then measured [2]. The applied methodology may differ in the acid used, the acid strength and the acidification time. The major sources of particle-bound TEs in ice cores are typically marine salts and mineral dust. While the salts are completely dissolved by the added acid, TEs in mineral dust are only partially leached, with the partitioning depending on the acidification time [3,4].

For the analysis of an ice core from Cerro Negro glacier (Chilean Andes, 4604 m asl.) performed in [1], the acid was added to the sample stream in front of the ICP-TOF-MS inlet system resulting in an acidification time of less than 1 min, while the samples were acidified between 1.5 h and 4 h prior to analysis with the ICP-SF-MS system. In this study, the effect of sample acidification time was tested, using ice from the same core. In the course of the test, 38 TEs were measured using an ICP-SF-MS (Element2, Thermo Scientific). The test was carried out on two days with an identical test set-up but different samples. Each day, five pre-cleaned tubes were filled with aliquots of the same sample. A calculated amount of 0.2 M HCl was then added to each tube at predetermined times. This allowed the following acidification times to be measured with three repetitions each: 1 min; 10 min; 20 min; 30 min; 1 h; 1.5 h; 2 h; 2.5 h; 3 h; 3.5 h and 4 h. The test showed changes in concentration over time for most TEs. While concentrations of some TEs remained constant (Ni, Zn, Sb, Co, Cu, Na), others showed opposite trends for the two samples (Li, Mo, Ag, Eu, Th, Ca, Mn). For the majority of TEs a significant change in concentration was observed. After 4 h of acidification time, changes ranged between -65 % and +164 %. Concentration increased by 10-50 % for Al, Sc, Cu, Rb, Sr, La, Pr and Bi; by 50-100 % for Cr, Fe, Ce, Nd, Sm and Pb and by >100 % for Mg and Ba. A decrease was recorded for some TEs, with -10 to -30 % for V and Tl; -30 to -50 % for Cd, Yb, and W; and >50 % for Zr. Previously performed acidification tests demonstrate that the change in concentration of the TEs is not only dependent on the acidification time, but also on the lithology of the mineral dust [2,3,4]. The solution of TEs from the minerals is related to their position in the crystal lattice and the mineral structure [3].

In our samples, the mineral dust consists mainly of albite, quartz and muscovite. Albite has a complex silicate structure in which TEs are relative tightly bonded. Therefore, contained TEs would be expected to dissolve rather slowly but steadily which could explain the observed continuous increase of e.g. Al concentrations over the tested time range. Meanwhile muscovite is a sheet silicate, with rather weak bonds between the sheets allowing TEs to dissolve quickly into the solution. Between the sheets Pb is often deposited, which release fast into the solution and this could be an explanation for the rise of Pb (Fig. 1). The decrease of some TEs (Zr, Tl, W, V, Yb, Cd) can be explained by hardly soluble compounds such as oxychlorides, forming in the acidified sample. These compounds strongly adsorb on surfaces and when thereby fixed to the sample tube walls might then no longer be available for analysis. The decrease in concentration could further be caused by the re-placement of dissolved ions in the crystal lattice. For example, Zr can replace Mg in hexagonal closed packed crystal structures.

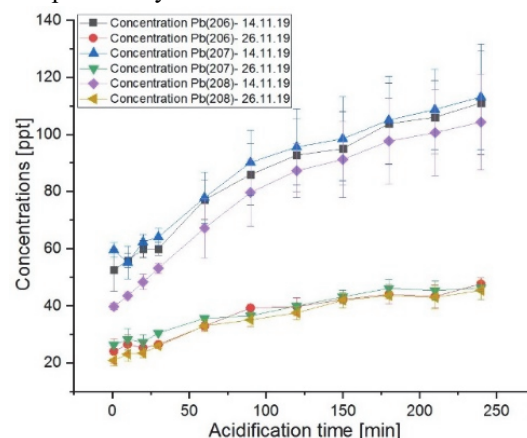


Fig. 1: Effect of sample acidification time on measured concentrations of Pb for two different ice samples. Each data point represents the mean of three replicate measurements, with the standard deviation shown by the error bar.

Our results show, that for most TEs, especially for lithophilic elements, the in [1] observed differences in concentrations determined by either the ICP-SF-MS or the ICP-TOF-MS system can be explained by the different acidification times used.

- [1] J. Stegmaier et al., Annual Report LUC, 25 (2018).
- [2] B. G. Koffman et al., *J. Glaciology*, **60**, 103-112, (2014).
- [3] C. Uglietti et al., *App. Geochemistry*, **47** 109-121 (2014).
- [4] R. H. Rhodes et al., *Chem. Geol.*, **286**, 207-221 (2011).

LIST OF PUBLICATIONS

SURFACE CHEMISTRY

- P. A. Alpert, P. Corral Arroyo, J. Dou, U. K. Krieger, S. S. Steimer, J.-D. Förster, F. Ditas, C. Pöhlker, S. Rossignol, M. Passananti, S. Perrier, C. George, M. Shiraiwa, T. Berkemeier, B. Watts, M. Ammann
Visualizing reaction and diffusion in xanthan gum aerosol particles exposed to ozone
Physical Chemistry Chemical Physics **21**, 20613-20627, doi: 10.1039/C9CP03731D
- T. Bartels-Rausch, M. Montagnat
The physics and chemistry of ice
Philosophical Transactions of the Royal Society A: Mathematical, Physical and Engineering Sciences **377** (2146), doi: 10.1098/rsta.2019.0138
- Q. Chen, J. Edebeli, S. M. McNamara, K. D. Kulju, N. W. May, S. B. Bertman, S. Thanekar, J. D. Fuentes, K. A. Pratt
HONO, particulate nitrite, and snow nitrite at a midlatitude urban site during wintertime
ACS Earth and Space Chemistry **3**, 811-822, doi: 10.1021/acsearthspacechem.9b00023
- P. Corral Arroyo, R. Aellig, P. A. Alpert, R. Volkamer, M. Ammann
Halogen activation and radical cycling initiated by imidazole-2-carboxaldehyde photochemistry
Atmospheric Chemistry and Physics **19**, 10817-10828, doi: 10.5194/acp-19-10817-2019
- J. Dou, B. Luo, T. Peter, P. A. Alpert, P. Corral Arroyo, M. Ammann, U. K. Krieger
Carbon dioxide diffusivity in single, levitated organic aerosol particles
The Journal of Physical Chemistry **10**, 4484-4489, doi: 10.1021/acs.jpcc.9b01389
- J. Edebeli, M. Ammann, T. Bartels-Rausch
Microphysics of the aqueous bulk counters the water activity driven rate acceleration of bromide oxidation by ozone from 289-245 K
Environmental Sciences: Processes and Impacts **21**, 63-73, doi: 10.1039/C8EM00417J
- M.-T. Lee, F. Orlando, M. Khabiri, M. Roeselová, M. A. Brown, M. Ammann
The opposing effect of butanol and butyric acid on the abundance of bromide and iodide at the aqueous solution-air interface
Physical Chemistry Chemical Physics **21**, 8418-8427, doi: 10.1039/C8CP07448H
- G. Li, Y. Cheng, U. Kuhn, R. Xu, Y. Yang, H. Meusel, Z. Wang, N. Ma, Y. Wu, M. Li, J. Williams, T. Hoffmann, M. Ammann, U. Pöschl, M. Shao, H. Su
Physicochemical uptake and release of volatile organic compounds by soil in coated-wall flow tube experiments with ambient air
Atmospheric Chemistry and Physics **19**, 2209-2232, doi: 10.5194/acp-19-2209-2019
- A. Liati, D. Schreiber, P. A. Alpert, Y. Liao, B. T. Brem, P. Corral Arroyo, J. Hu, H. R. Jonsdottir, M. Ammann, P. Dimopoulos Eggenschwiler
Aircraft soot from convention fuels and biofuels during ground idle and climb-out conditions: Electron microscopy and X-ray micro-spectroscopy
Environmental Pollution **247**, 658-667, doi: 10.1016/j.envpol.2019.01.078
- F. Orlando, L. Artiglia, H. Yang, X. Kong, K. Roy, A. Waldner, S. Chen, T. Bartels-Rausch, M. Ammann
Disordered adsorbed water layers on TiO₂ nanoparticles under subsaturated humidity conditions at 235 K
The Journal of Physical Chemistry Letters **10**, 7433-7438, doi: 10.1021/acs.jpclett.9b02779
- J. L. Thomas, J. Stutz, M. M. Frey, T. Bartels-Rausch, K. Altieri, F. Baladima, J. Browse, M. Dall'Osto, L. Marelle, J. Mougino, J. G. Murphy, D. Nomura, K. A. Pratt, M. D. Willis, P. Zeiger, J. Abbatt, T. A. Douglas, M. C. Facchini, J. France, A. E. Jones, K. Kim, P. A. Matrai, V. Faye McNeill, A. Saiz-Lopez, P. Shepson, N. Steiner, K. S. Law, S. R. Arnold, B. Delille, J. Schmale, J. E. Sonke, A. Dommergue, D. Voisin, M. L. Melamed, J. Gier
Fostering multidisciplinary research on interactions between chemistry, biology, and physics within the coupled cryosphere-atmosphere system
Elementa: Science of the Anthropocene **7**, 16 pp., doi: 10.1525/elementa.396

ANALYTICAL CHEMISTRY

- S. E. Avak, J. C. Trachsel, J. Edebeli, S. Brüttsch, T. Bartels-Rausch, M. Schneebeli, M. Schwikowski, A. Eichler
Melt-induced fractionation of major ions and trace elements in an alpine snowpack
Journal of Geophysical Research F: Earth Surface, **124**, 1647-1657, doi: 10.1029/2019JF005026
- S. O. Brügger, E. Gobet, T. Blunier, C. Morales-Molino, A. F. Lotter, H. Fischer, M. Schwikowski, W. Tinner
Palynological insights into global change impacts on Arctic vegetation, fire and pollution recorded in Central Greenland ice
The Holocene **29**, 1189-1197, doi: 10.1177/0959683619838039
- S. O. Brügger, E. Gobet, D. Osmont, H. Behling, S. L. Fontana, H. Hooghiemstra, C. Morales-Molino, M. Sigl, M. Schwikowski, W. Tinner
Tropical Andean glacier reveals colonial legacy in modern mountain ecosystems
Quaternary Science Reviews **220**, 1-13, doi: 10.1016/j.quascirev.2019.06.032
- S. O. Brügger, E. Gobet, F. R. Schanz, O. Heiri, C. Schwörer, M. Sigl, M. Schwikowski, W. Tinner
Why loss matters: Reply to the comments of Festi and others on 'A quantitative comparison of microfossil extraction methods from ice cores' by Brügger and others (2018)
Journal of Glaciology **65**, 867-868, doi: 10.1017/jog.2019.61
- K. R. Daellenbach, I. Kourtchev, A. L. Vogel, E. A. Bruns, J. Jiang, T. Petäjä, J.-L. Jaffrezo, S. Aksoyoglu, M. Kalberer, U. Baltensperger, I. El Haddad, A. S. H. Prévôt
Impact of anthropogenic and biogenic sources on the seasonal variation in the molecular composition of urban organic aerosols: a field and laboratory study using ultra-high-resolution mass spectrometry
Atmospheric Chemistry and Physics **19**, 5973-5991, doi: 10.5194/acp-19-5973-2019
- L. Fang, J. Schindler, T. M. Jenk, C. Uglietti, S. Szidat, M. Schwikowski
Extraction of dissolved organic carbon from glacier ice for radiocarbon analysis
Radiocarbon **61**, 681-694, doi: 10.1017/RDC.2019.36
- M. Hartmann, T. Blunier, S. O. Brügger, J. Schmale, M. Schwikowski, A. Vogel, H. Wex, F. Stratmann
Variation of ice nucleating particles in the European arctic over the last centuries
Geophysical Research Letters **46**, 4007-4016, doi: 10.1029/2019GL082311
- S. Hou, W. Zhang, H. Pang, S.-Y. Wu, T. M. Jenk, M. Schwikowski
Apparent discrepancy of Tibetan ice core $\delta^{18}O$ records may be attributed to misinterpretation of chronology
The Cryosphere **13**, 1743-1752, doi: 10.5194/tc-13-1743-2019
- A. C. F. King, C. Giorio, E. Wolff, E. Thomas, M. Roverso, M. Schwikowski, A. Tapparo, S. Bogialli, M. Kalberer
Direct injection liquid chromatography high-resolution mass spectrometry for determination of primary and secondary terrestrial and marine biomarkers in ice cores
Analytical Chemistry **91**, 5051-5057, doi: 10.1021/acs.analchem.8b05224
- A. C. F. King, C. Giorio, E. Wolff, E. Thomas, O. Karroca, M. Roverso, M. Schwikowski, A. Tapparo, A. Gambaro, M. Kalberer
A new method for the determination of primary and secondary terrestrial and marine biomarkers in ice cores using liquid chromatography high-resolution mass spectrometry
Talanta **194**, 233-242, doi: 10.1016/j.talanta.2018.10.042
- D. Osmont, M. Sigl, A. Eichler, T. M. Jenk, M. Schwikowski
A Holocene black carbon ice-core record of biomass burning in the Amazon Basin from Illimani, Bolivia
Climate of the Past **15**, 579-592, doi: 10.5194/cp-15-579-2019
- J. C. Trachsel, S. E. Avak, J. Edebeli, M. Schneebeli, T. Bartels-Rausch, S. Brüttsch, A. Eichler
Microscale rearrangement of ammonium induced by snow metamorphism
Frontiers in Earth Science **7**, 19 pp., doi: 10.3389/feart.2019.00194
- A. L. Vogel, A. Lauer, L. Fang, K. Arturi, F. Bachmeier, K. R. Daellenbach, T. Käser, A. Vlachou, V. Pospisilova, U. Baltensperger, I. El Haddad, M. Schwikowski, Saša Bjelić
A comprehensive nontarget analysis for the molecular reconstruction of organic aerosol composition from glacier ice cores
Environmental Sciences & Technology, **53**, 12565-12575, doi: 10.1021/acs.est.9b03091

AFFILIATION INDEX

Aix-Marseille Univ.	Aix-Marseille Université, Jardin du Pharo, 58, boulevard Charles Livon, 13284 Marseille Cedex 07, France
ASI	Abteilung Strahlenschutz und Sicherheit, Paul Scherrer Institut, 5232 Villigen, Switzerland
BAdW	Bayrische Akademie der Wissenschaften, Alfons-Goppel-Strasse 11, 80539 München, Germany
CECs	Centro de Estudios Científicos, Arturo Prat 514, Valdivia, Chile
EMPA	Materials Science and Technology, Überlandstrasse 129, 8600 Dübendorf, Switzerland
ENE	Energy and Environment Division, Paul Scherrer Institut, 5232 Villigen, Switzerland
ETHZ	ETH Zurich, Eidgenössische Technische Hochschule Zürich, 8092 Zürich, Switzerland
Indiana Univ.	Indiana University Bloomington, 107 S. Indiana Avenue, Bloomington, IN 47405-7000, USA
IRCELYON, CNRS	Institut de Recherches sur la Catalyse et l'Environnement de Lyon, 2 avenue Albert Einstein, 69626 Villeurbanne cedex, France
JLJU	Jilin Jianzhu University, Changchun, 130118, China
LEC	Laboratory for Electrochemistry, Paul Scherrer Institut, 5232 Villigen, Switzerland
LMN	Laboratory for Micro and Nanotechnology, Paul Scherrer Institut, 5232 Villigen, Switzerland
LRT	Laboratory for Reactor Physics and Thermal-Hydraulics, Paul Scherrer Institut, 5232 Villigen, Switzerland
LSC	Laboratory for Condensed Matter, Paul Scherrer Institut, 5232 Villigen, Switzerland
LSF	Laboratory for Synchrotron Radiation and Femtochemistry, Paul Scherrer Institut, 5232 Villigen, Switzerland
LSK	Laboratory for Catalysis and Sustainable Chemistry, Paul Scherrer Institut, 5232 Villigen, Switzerland
LUC	Laboratory of Environmental Chemistry, Paul Scherrer Institut, 5232 Villigen, Switzerland
MPIC	Max-Planck-Institut für Chemie, Hahn-Meitner-Weg 1, 55128 Mainz, Germany
NES	Nuclear Energy and Safety Division, Paul Scherrer Institut, 5232 Villigen, Switzerland
NUIST	Nanjing University of Information Science and Technology, No. 219, Ningliu Road, Nanjing, Jiangsu, China
PKU	Peking University, No. 5 Yiheyuan Road, Haidian District, Beijing 100871, China
PSD	Photon Science Division, Paul Scherrer Institut, 5232 Villigen, Switzerland
PSI	Paul Scherrer Institut, Forschungsstrasse 111, 5232 Villigen, Switzerland
QEERI	Hamad Bin Khalifa University, Qatar Environment and Energy Research Institute, Education City, Doha, Qatar
THU	Tsinghua University, Haidian District, Beijing, 100084, China
TUM	Technische Universität München, Arcisstraße 21, 80333 München, Deutschland
unibz	Libera Università di Bolzano, piazza Università, 5, 39100 Bolzano, Italy
Univ. Basel	Universität Basel, Departement Umweltwissenschaften, Klingelbergstrasse 27, 4056 Basel, Switzerland
Univ. Bern	Universität Bern, Departement für Chemie und Biochemie, Freiestrasse 3, 3012 Bern, Switzerland
Univ. California	University of California, Irvine, CA 92697, USA
Univ. Fribourg	Université de Fribourg, Avenue de l'Europe 20, 1700 Fribourg, Switzerland
Univ. Helsinki	University of Helsinki, Fabianinkatu 33, 00014 University of Helsinki, Finland
Univ. Milano	Università degli Studi di Milano-Bicocca, Piazza dell'Ateneo Nuovo, 1, 20126 Milano, Italy
Univ. Nanjing	Nanjing University, School of Geographic & Oceanographic Sciences, Hankou Road 22, Nanjing, Jiangsu, China
Univ. Torino	Università degli Studi di Torino, Via Verdi, 8, 10124 Torino, Italy
UZH	University of Zurich, Department of Geography, Winterthurerstrasse 190, 8057 Zürich, Switzerland
WSL-SLF	Swiss Federal Institute for Forest, Snow and Landscape Research WSL, 8903 Birmensdorf, Switzerland

